Searching for Binary and Millisecond Pulsars: A High-Latitude Drift-Scan Survey

by

Laura Elizabeth Kasian

B.Sc., The University of Winnipeg, 2003

A THESIS SUBMITTED IN PARTIAL FULFILMENT OF
THE REQUIREMENTS FOR THE DEGREE OF

Master of Science

in

The Faculty of Graduate Studies

(Astronomy)

The University Of British Columbia

October, 2005

Abstract

We performed a drift-scan pulsar survey using the Green Bank Telescope (GBT) in West Virginia, USA. The survey is among the most sensitive ever undertaken in the Northern sky, and was collected with the Berkeley-Caltech Pulsar Machine filterbank. It was performed at low frequencies (400, 600, and 800 MHz) and mostly high Galactic latitudes with the aim of detecting new binary and millisecond pulsars. Population models of pulsars have shown that young pulsars tend to be concentrated in the Galactic plane, while binary and millisecond pulsars appear to have a more isotropic distribution on the sky. Searches at high Galactic latitudes are therefore required in order to discover new binary and millisecond pulsars, and to better understand the distinct population of millisecond (recycled) pulsars. The data from the survey were reduced mainly using the `sigproc` pulsar signal processing software package. As of the writing of this thesis, $\sim 73\%$ of the data have been searched for periodicities. Each pulsar candidate is given a classification based on how closely it resembles a pulsar (Class 1 = probably a pulsar; Class 4 = most likely not a pulsar) . We were successful in re-detecting 4 previously-known pulsars, and we obtained lists of Class-1 and Class-2 candidates. We will confirm these candidates through follow-up observations with the GBT in December 2005. We detected fewer convincing Class 1 candidates than expected, which we attribute to a recently-discovered problem in the `sigproc` software and persistent radiofrequency interference (RFI) in the data, particularly at 600 MHz. We have corrected the software problem, which has resulted in the discovery our first Class-1 pulsar candidates. We expect that a reanalysis of processed scans and a first analysis of the remaining $\sim 27\%$ of data will yield a significantly higher number of promising candidates.

Contents

List of Tables

List of Figures

Chapter 1

Introduction

Pulsars are interesting objects, allowing us to study neutron stars with extreme precision. They can act as unique probes into extreme regimes of physics, and can help us understand stellar evolution. As the most stable clocks in nature, pulsars provides some of the most precise astronomical data available. However, before any science can benefit from the study of pulsars, we must first rise to the occasion of locating new pulsars. Searching for new pulsars is not a trivial exercise. Large volumes of data as well as computationally intensive calculations are required, and many hours of telescope time and state-of-the-art hardware are also needed. However, the payoff from searching for pulsars can be very exciting. Exotic binary pulsars such as double neutron-star systems can be highly relativistic systems, thereby providing testing grounds for strong-field gravity. Similarly, the discovery of a pulsar with mass unambiguously greater than two solar masses (c.f. Nice et al. 2005), or a pulsar with a sub-millisecond spin period could constrain the set of theories allowed for the neutron star equation-of-state.

1.1 Radio Pulsars - Overview

The study of pulsars has come a long way since their initial discovery by Bell and Hewish in 1967 (Hewish et al. 1968). When the first pulsar was detected, the regularity of its pulses was the most striking feature. It was not immediately obvious that there existed a natural phenomenon that could emit such a regularly pulsed signal, and it was even considered that the signal could be a transmission from extraterrestrial intelligent life. Soon after the initial discovery, however, Pacini (1968) and Gold (1968) independently put forth the idea that the pulsar emission originates from rapidly rotating, highly magnetised neutron stars. In fact, Pacini (1967) had postulated two years prior that a magnetized neutron star could power the Crab nebula. In 1968, the pulsar in the Crab nebula was discovered (Staelin and Reifenstein), which strengthened the case for the neutron star theory. However, at

the time of the initial pulsar discovery, neutron stars were known to theorists but were obscure to observers. Neutron stars were first proposed in 1934 by Baade and Zwicky, who had acknowledged that a possible result of a supernova explosion is a small, massive star consisting mainly of neutrons. There were many other ideas proposed to explain the pulsar phenomenon. Theories involving more familiar white dwarfs were favored by some observers. Also, it was not immediately clear that the pulsations were from rotation. Two competing explanations involved stellar oscillations and the orbital motion of an extremely low-mass companion about a massive star (eg, Lyne and Graham-Smith 1998). The discovery of the Crab and Vela pulsars ruled out the possibility that oscillations were responsible for the pulsations. The periods of these pulsars (33ms and 89ms, respectively) fell in a gap between the expected oscillation frequency for neutron stars and that for white dwarfs. The orbital theory was also shown to be extremely unlikely to produce the stable pulsations seen in the observed pulsars. Rotation or vibration seemed to be the only likely explanation for the pulses. The discovery that the Crab pulsar slows down with time (Richards and Comella 1969) finally limited the choice to the rotation scenario, as neutron star rotation is expected to slow down with time, while the vibrations are not. It is currently widely believed that the pulsars are rapidly rotating neutron stars.

1.1.1 Integrated Profiles

We study pulsars is though a *time series*, a series of voltages sampled at a certain sampling rate, t_{samp}. The time series of a typical pulsar has pulsations that are regularly spaced at the spin period of the neutron star (with the exception of *nulling* pulsars (Backer, 1970), and some pulsars exhibiting subpulses (Drake and Craft 1968)). Although the individual pulses of some pulsars can be seen by eye in the time series, most pulsars do not have individual pulses that are visible above the noise background of the receiver. In order to gain any useful information about the neutron star and its environment, it is a common practice (once the period of the pulsar is determined) to *fold* the time series at the spin period. Folding the data consists of adding the pulsar power modulo the topocentric period (i.e., the period of the pulsar as seen by the receiver). The signal increases approximately linearly with the number of pulses n_p; i.e., $S \propto n_p$, while the the noise increases as $N \propto \sqrt{n_p}$. The signal-to-noise ratio (SNR) therefore increases as $SNR \propto \sqrt{n_p}$. Since the number of pulses increases linearly with time, $SNR \propto \sqrt{time}$. The *integrated profile* of a pulsar is the

result of folding its signal at the topocentric period.
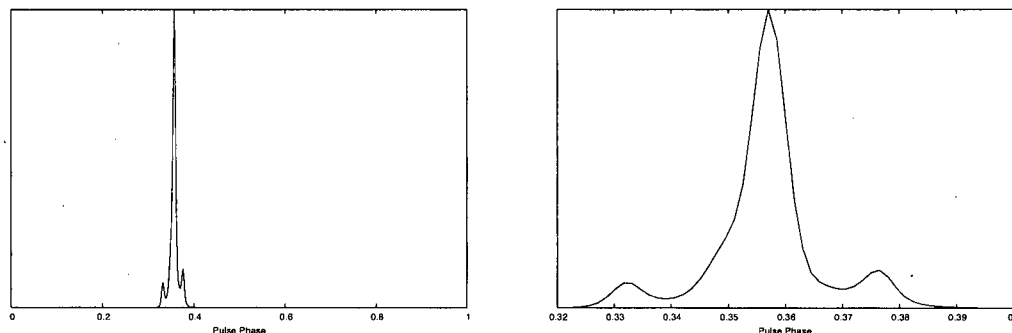
Figure 1.1: An example of an integrated profile, created using data from the EPN database (*http://www.mpifr-bonn.mpg.de/div/pulsar/data/browser.html*). This is a 600-MHz signal of PSR B0329+54, from Gould and Lyne (1998). The plot on the left shows the entire pulse phase. The plot on the right zooms in on the pulse.

For a given time series, the shape of each individual pulse varies from one pulse to the next. However, once an integrated profile is created by summing several thousand pulses, the shape of the profile is generally stable with no detectable long-term variations (Helfand et al. 1975). Although this is true for most pulsars, there are exceptions, including some double neutron star (DNS) systems in which profile changes are seen over long-term measurements due to geodetic precession (e.g., Weisberg et al. 1989), and some isolated pulsars apparently showing free precession (Stairs et al. 2000). The duty cycle of a normal pulsar is typically between 2-5% (Hankins and Rickett 1975), but millisecond pulsars have significantly higher duty cycles, which can be up to $\sim 30\%$ (Kramer et al. 1998). The shape of the pulse profile of MSPs are also, on average, slightly more complex. Using a sample of 180 pulsars, Kramer et al. (1998) determined that the median number of components required to represent the profiles of normal pulsars is 3, while the MSPs can be described by 4.

The shape of the integrated profile is thought to contain information about the pulse emission mechanism at the polar regions of the neutron star. There are several simple models of the radio emission beam. Although these models can help explain and predict the emission properties of pulsars, they are empirical models - a firm theoretical understanding of the pulsar magnetosphere and emission mechanism is still lacking. The geometry of

the emission beam is often modeled as a hollow cone centered about the magnetic axis of the neutron star, and was suggested early on by Radhakrishnan and Cooke (1969) and Komesaroff (1970). This model can somewhat account for the multiple components within the integrated profiles: we see more emission when our line-of-sight passes through the outer edge of the emission cone, and we see a drop in emission when we are not looking directly along an edge. If, as the neutron star rotates, our line-of-sight happens to slice through the cone, then we will see two edges and therefore two components. We see only one component if our line-of-sight happens to be right at the edge of the emission cone. In order to account for more complex emission beams, Backer (1976) extended this idea to include a *core* component in the centre of a hollow emission cone. Others further included nested cones (eg. Rankin 1993) in order to allow for yet more complex profiles. As an alternative to the cone-core model, Lyne and Manchester (1988) suggested a 'patchy beam' model for the emission beam. In this model, random regions of open field lines emit radiation, making for a patchy emission region that can account for more complex profiles better than the nested cone model. However, the patchy beam model does not explain the evolution of the profile with frequency as well as the nested cone model. Although these models can help understand some aspects of the pulsar emission process, there are still many open questions that need to be answered before we can understand it more completely. In particular, the coherent radiation process responsible for the observed radio emission is still not understood.

1.1.2 Dispersion

Dispersion by the interstellar medium plays a fundamental role in the study of pulsars. Generally, when an integrated profile is created for a given pulsar, we sum not only over all sub-integrations in the time series, but also over a range of frequencies. Although the emission mechanism for radio pulsars is still a heavily debated topic, it is commonly assumed that each pulse is emitted from the emission cone of the neutron star nearly simultaneously at all radio frequencies within a given, relatively narrow bandwidth. However, the radiation from each pulse is *dispersed* by the interstellar medium that lies between the Earth and the pulsar. Dispersion introduces a relative delay in the pulsar's signal between high- and low-observing frequencies. Over a range of frequencies from ν_1 and ν_2 we observe a relative delay of:

$$\Delta t = \frac{1}{2.41 \times 10^{-4} \ s^{-1}} \times (\nu_1^{-2} - \nu_2^{-2}) \cdot DM \quad (1.1)$$

$$DM = \int_0^z N_e dz$$

where DM is the *dispersion measure* of the pulsar, equal to the integral of the electron density N_e along the propagation path (eg, Hankins and Rickett 1975). See Figure 1.2 for an example of a dispersed signal. Although the effect of dispersion is second-order in frequency, for the purpose of searching it often suffices to approximate this effect as linear over a small range of frequencies. For a more formal discussion of dispersion, including the propagation of the pulsar signal considering the transfer function of the interstellar medium, see Hankins and Rickett (1975).

Not only can dispersion be seen between individual frequency channels (as in Figure 1.2), but it also has implications for the pulse shape itself. Within a given channel of bandwidth $\Delta \nu$, the pulse will be a sum of all frequencies within the bandwidth. In fact, the pulse will be smeared over a time interval , which can be approximated as (eg, Lyne and Graham-Smith 1998):

$$\tau_{DM} \approx 8.3 \times 10^3 \frac{DM}{\nu_{MHz}^3} \Delta \nu \ sec \qquad (1.2)$$

In order to minimize the effect of dispersion smearing within a given bandwidth, the simplest solution is to split the bandwidth into many narrow channels. When this is done, it is possible to improve the signal-to-noise ratio of the pulsar by correcting for the relative delay of the pulsar's signal at different frequencies. This process is called *dedispersion* and will be discussed in more detail in §1.1.2. If the DM of the pulsar is known, then we add an appropriate time delay to the time series at each frequency channel (as in equation 1.1), and then sum all frequency channels. Dedispersion can dramatically increase the signal-to-noise ratio. The effect is illustrated in Figure 1.2: if the time series at each frequency were added up without adding a time delay, all the individual pulses would not add coherently, and would thus produce no net signal. However, when the data is dedispersed before summing over all frequencies channels, we obtain the pulse shown at the bottom of the figure.

1.2 Binary and Millisecond Pulsars

1.2.1 Millisecond Pulsars versus Normal Pulsars

There are about 1600 radio pulsars known to date. The spin periods range from 8.5 seconds (Young et al. 1999) for the slowest known pulsar to 1.558 milliseconds (Backer et al. 1982)
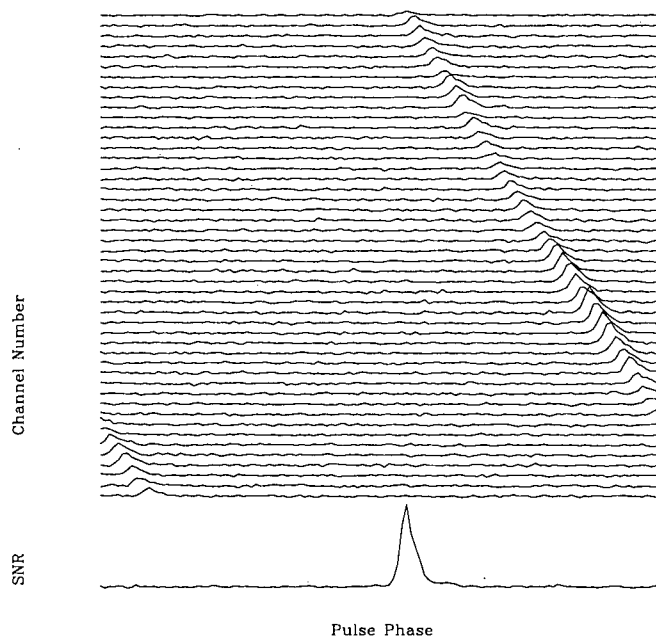
Figure 1.2: 130 s observation of J1518+4904 using the GBT. The x-axis is the pulse phase, and the y-axis is the sub-band number. We have plotted the (dedispersed) folded time series for 48 sub-bands, with the centre observing frequency being 590 MHz. The integrated profile is shown at the bottom of the plot. The period and dispersion measure of this pulsar, respectively, are ~ 40.9447 ms and 11.7 $cm^{-3}pc$.

for the fastest. If we plot a histogram of the spin periods of known pulsars (see Figure 1.3), we notice that the distribution is bimodal. The smaller, more rapidly-spinning population is what is now known as the class of *millisecond* pulsars (MSPs). The slower pulsars are referred to as *normal* pulsars. The first millisecond pulsar to be discovered, B1937+21 (Backer et al. 1982), is currently still the fastest pulsar known.

It has become clear that the population of millisecond pulsars is phenomenologically different from that of normal pulsars. Within a year of the discovery of the first MSP, both Alpar et al. (1982) and Radhakrishnan and Srinivasan (1982) had suggested accreting binary systems (in particular, the low-mass X-ray binaries, or LMXBs) as a progenitor for
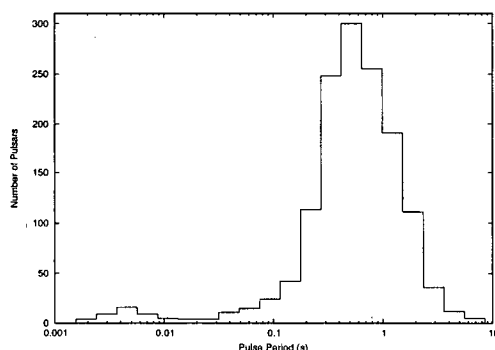
Figure 1.3: A histogram of the periods of a large sample of the known pulsars. Pulsars detected in globular clusters are omitted. Notice the bimodality of the distribution that distinguishes the two populations, normal and millisecond classes. Data from the ATNF pulsar catalogue (Hobbs et al. 2004, http://www.atnf.csiro.au/research/pulsar/psrcat/)

MSPs. LMXBs are close binary systems in which a neutron star accretes matter from a low-mass companion, and X-rays are emitted due to gravitational interactions of infalling material onto the neutron star's surface. During this stage, the companion has evolved into a giant, filling its Roche lobe and transferring matter and angular momentum onto the neutron star. This causes the neutron star to be spun up or 'recycled' to a millisecond rotation period by the end of the accretion process. Through some (currently) unknown mechanism, the magnetic field of the neutron star, and hence the spin-down rate of the pulsar, become low. This gives the millisecond pulsar an extremely stable rotational period. The argument for this accretion scenario has recently been strengthened by the detection of millisecond oscillations in LMXB systems. In 1996, observations of two types of quasi-periodic oscillations were detected in LMXBs, whose oscillation frequencies hinted towards a connection to MSPs. In 1996, kilohertz quasi-periodic oscillations (kHz QPOs) were seen in Sco X-1 by Van Der Klis et al. (1996), and in 4U 1728-34 by Strohmayer et al. (1996). These oscillations were interpreted as a beat-frequency between the neutron star rotation period and the orbital frequency of accretion-disk material around the neutron star. During the same year, oscillations were detected in 4U 1738-34 (Strohmayer et al. 1996) during a Type-I X-ray burst (a type of burst that is attributed to a thermonuclear flash on the surface of an

accreting neutron star). The burst was modulated by a frequency that initially increased but asymptotically approached a single value in the tail of the burst. The oscillation was thought to be related to the neutron star spin period. In 1998, a detection was finally made of coherent oscillations within the persistent emission of an LMXB. The transient X-ray source SAX J1808.4-3658 exhibited 2.49 millisecond oscillations which showed a clear periodicity, highly stable to within 0.01%, at the spin frequency of the accreting neutron star (Wijnands and van der Klis 1998). Further, in 2003 burst oscillations were also seen in J1808.4-3658 (Chakrabarty et al. 2003) at the spin period of the neutron star, as determined by the coherent oscillations in 1998. Kilohertz QPOs were also detected in the millisecond X-ray pulsars J1808.4-3658 (Wijnands et al., 2003) and XTE J1807-294 (Linares et al., 2005). These discoveries effectively closed the observational gap between the LMXBs and MSPs, by providing evidence that neutron stars within LMXBs are able to spin at very fast periods.

The term 'millisecond pulsar' has come to include those with periods from 1.5 to 30 ms, more or less. It refers to pulsars that have been spun up or recycled through the process described here, which typically have spin periods in the aforementioned range. The heavily recycled MSPs (i.e. those that have been spun up to very low spin periods) are thought to be those with LMXB progenitors; however, more massive systems (eg, double neutron star systems) which are not as recycled are still included as MSPs.

1.2.2 Millisecond Pulsars and the $P - \dot{P}$ diagram

It is useful to look at a '$P - \dot{P}$' diagram such as in Figure 1.4 in order to understand, at least observationally, the difference between the two populations of pulsars. It is clear that there are two distinct islands of pulsars within the period-period derivative space: the normal pulsars are concentrated in the middle-to-upper right area of the plot, while millisecond pulsars appear towards the lower left-hand corner.

We can gain a rough idea of the magnetic field B and the characteristic age τ of a pulsar from its position on the $P - \dot{P}$ diagram. Since the pulsar has a strong dipole magnetic field, it is convenient to make the assumption that it is a perfect magnetic dipole. If we assume the spin-down luminosity of the pulsar is strongly dominated by dipole radiation, we can

obtain an expression for the surface magnetic field B of the pulsar:

$$B_S = \sqrt{\frac{3c^3}{8\pi^2} \frac{I}{R^6 \sin^2 \alpha} P\dot{P}} \qquad (1.3)$$

(eg, Lorimer and Kramer 2004). For a neutron star that has radius R = 10 km, moment of inertia I = 10^{45} g cm^2, and orthogonal spin and magnetic axes (i.e., $\alpha = \pi$), we obtain the following:

$$B_S = 3.2 \times 10^{19} \, G \times \sqrt{P\dot{P}} \qquad (1.4)$$

If we assume that the spin frequency ν and frequency derivative $\dot{\nu}$ follow a general power law with index n, $\dot{\nu} = -K\nu^n$, then in terms of the period P and period derivative $\dot{P}$ we can write, $\dot{P} = KP^{2-n}$. Integrating this expression over time, we obtain the following characteristic age of a pulsar born with period P_0:

$$T = \frac{P}{(n-1)\dot{P}} \left[1 - \left(\frac{P_0}{P} \right)^{n-1} \right] \qquad (1.5)$$

(eg, Lorimer and Kramer 2004). If we include the assumption that a dipole magnetic field is the dominant source of rotational energy loss in the pulsar, then we have the braking index $n = 3$. If we also assume also that $P_0 << P$, then Equation 1.5 simplifies to:

$$\tau_c = \frac{P}{2\dot{P}} \qquad (1.6)$$

The characteristic age is often not a good estimation of the true age of a pulsar. For example, Camilo et al. (1994) found that the characteristic ages of some millisecond pulsars exceeded the age of the galactic disk, which does not make sense. However, τ_c is still a useful quantity to measure, since there is often no better estimate available. It is possible to measure the braking index n in systems where measurements of the second period derivative are available, and provided we are confident it is not timing noise. This can then be compared with the value of 3 which is assumed in the case of a magnetic dipole. For rotation frequency Ω, the braking index can be expressed as $n = \Omega\ddot{\Omega}/\dot{\Omega}^2$.

We now have a rough estimate for the surface magnetic field B_S of the pulsar, and its characteristic age τ_c . Both are related to the period and period derivative through a power law. When we plot curves of constant characteristic age and of constant surface magnetic

field, they appear on the log-log $P - \dot{P}$ diagram as lines. In Figure 1.4, lines are plotted for several values of constant τ_c and B_S.

Young pulsars begin their lives in the top left region of the plot. As the pulsar radiates away rotational energy and loses angular momentum, its period increases to somewhere near the largest island of pulsars in the plot, with typical periods on the order of one second, and typical spin-down rate of 10^{-15} s s^{-1} (eg. Lorimer 2001). After many ($\sim 10^8$) years, the pulsar has slowed down to a period that no longer suffices to produce the electron-positron pairs that provide the polar emission of radiation. We can no longer see the neutron star as a pulsar, and this region of the $P - \dot{P}$ space is often called the pulsar graveyard (Chen and Ruderman 1993).

The millisecond pulsar population are those that have been spun up to very stable, fast rotational periods. It is clear from the position of the millisecond pulsars in Figure 1.4 that they are a substantially older population with lower magnetic fields than normal pulsars. Typical millisecond pulsars have magnetic fields $\sim 10^8$ Gauss and characteristic ages of $\sim 10^9$ years. By comparison, normal pulsars have typical magnetic fields of $\sim 10^{12}$ Gauss, and characteristic ages of $\sim 10^{10}$ years (eg. Lorimer 2001). During the accretion process described above, the pulsar is thought to move in the diagram from below the death line to the lower left-hand corner, where it will remain for a long time due to its low period derivative.

1.2.3 Associations Between Binary and Millisecond Pulsars

Millisecond pulsars are much more likely than normal pulsars to have a binary companion. This is advantageous for learning about the supernova and mass-transfer histories of these systems: the vast majority of MSPs are in binary systems (around 80% of the observed MSPs have binary companions, as compared to less than one percent for normal pulsars (Lorimer 2001)), which means we can learn more about MSPs than about isolated pulsars. Through timing, the orbital parameters can be obtained, which provide clues as to how these systems formed. For example, in long-orbit low-mass MSP binaries, the theory of a red giant overflowing its Roche lobe and transferring matter to its companion through accretion, in combination with nonuniform plasma density within the envelope of the red giant, has been able to predict the orbital eccentricities of the systems fairly well (Phinney 1992; c.f. Stairs et al. 2005).
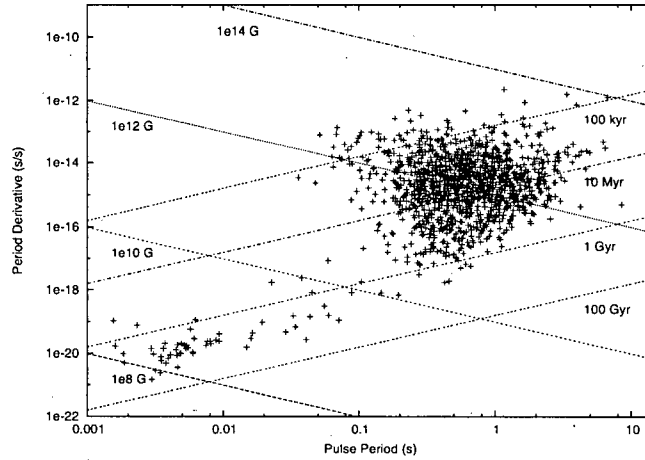
Figure 1.4: A $P - \dot{P}$ diagram, which plots the period derivative (or spin-down rate) of each pulsar versus its spin period. Data from the ATNF pulsar catalogue (Hobbs et al. 2004, http://www.atnf.csiro.au/research/pulsar/psrcat/. Pulsars in globular clusters are omitted.

Millisecond pulsars in binary systems can be extremely useful to study. They have extremely stable rotation periods, which makes them a valuable resource in testing general relativity (eg. Stairs 2003). However, only around 90 millisecond pulsars are currently known, many of them having been discovered in globular clusters (in which it is much more likely for the MSPs to interact with other systems than the rest of the MSP population). One of the goals of pulsar astronomy has therefore been to increase the known sample of millisecond and binary pulsars for further study.

1.2.4 The Galactic Distribution of Millisecond Pulsars

In order to further study millisecond pulsars, we must increase our sample; however, to do this we first need to know where to find them. Studies of the known population of MSPs can be used to guide our our surveys towards detecting new ones. The first MSP discovered at a high galactic latitude (Wolszczan 1990) provided evidence that the distribution of observable MSPs is roughly isotropic. This is a contrast from the population of young pulsars, which

are concentrated in the Galactic plane where they are born. Also, the inferred flux density S_ν for each pulse is related to the observing frequency ν by a power law $S_\nu \propto \nu^\alpha$. with typical spectral index $\alpha = -2$ (eg, Lorimer and Kramer 2004) or $\alpha = -1.6$ (Lorimer et al., 1995) so that pulsars are brighter at low frequencies. It was soon suggested (Johnston and Bailes 1991) that all-sky surveys at low frequencies would be an efficient way to discover new MSPs. Since then, many surveys at high- and intermediate- galactic latitudes have been performed, and have discovered ~ 50 MSPs (eg. Lorimer et al. 2005).

Population statistics of currently-known samples of pulsars have suggested that the number of active normal pulsars in the Galaxy is approximately equal to the number of active MSPs in the Galaxy (Lyne et al. 1998). However, MSPs are often heavily selected against in surveys. The average luminosity of MSPs appears to be lower than for normal pulsars. Also, DM smearing due to inadequate time sampling and/or coarse channelization has made them difficult to detect. In addition, acceleration within the binary systems we hope to discover creates another selection effect. Also, many surveys have concentrated on the Galactic plane, which is not the most efficient way to search for MSPs, as mentioned above.

It is clear that a high-latitude, extremely sensitive survey conducted at low frequencies would have the potential to discover new millisecond pulsars quite efficiently. We have conducted such a survey with the Green Bank Telescope, which will be discussed in more detail in Chapter 2.

Chapter 2

Pulsar Surveys and the GBT Drift-Scan Survey

2.1 Previous High-Latitude Surveys of the Northern Sky

There have been several groups who have undertaken high-latitude surveys of the Northern sky in the search for new MSPs in the past two decades. Four of these surveys are briefly outlined here.

- A survey at 411 MHz was performed using the 76-metre Lovell telescope at Jodrell Bank (Nicastro et al. 1995). This survey detected both circular polarizations, and used 8 MHz of total bandwidth which was split into 64 channels of 125 kHz each. The data was one-bit sampled at a rate of 0.3 ms. The survey yielded only one pulsar, PSR J1012+5307, which is a fast MSP in a 14.5 hour binary orbit around a white dwarf (Callanan et al. 1998; van Kerkwijk et al. 1996). The sensitivity to millisecond pulsars was 5 mJy.

- A 81.5-MHz survey was undertaken using the same Cambridge 3.6 Hectare dipole array that discovered the first pulsars (Shrauner et al. 1998). The array was operated as a total-power phased array, and had a total bandwidth of 1MHz and one-bit sampling at a rate of once per 0.768 ms. Declinations between $-20°$ and $+86°$ were surveyed. The survey was successful at re-detecting 20 previously-known pulsars, but did not discover any new ones. The survey was sensitive to MSPs down to 200 mJy.

- A search was performed at 390 MHz using the 92-m telescope at Green Bank (Dewey et al. 1985). This survey covered ~ 1.8 sr of the Northern sky, and sought to detect low-luminosity pulsars. The survey resulted in the detection of 83 pulsars, including 34 new ones. The bandpass of 16 MHz was split into 8 channels, at a sampling rate of

60 Hz. This survey was not sensitive to MSPs with periods below 30 ms. A companion survey (Stokes et al. 1986) was sensitive to MSPs but covered primarily the Galactic plane.

- A survey at 370 MHz was performed using the Green Bank 140-foot telescope (Sayer et al. 1997). The survey had a bandwidth of 40MHz and sampled once every 0.256 ms. Its sensitivity to MSPs was 8 mJy. Its goal was to detect the strongest millisecond pulsars in the Northern sky, and it succeeded in detecting 8 new pulsars including two recycled pulsars, PSR J0122+1001 (detected first by Camilo et al. (1996a)) and PSR J1518+4904 (Nice et al. 1996). 76 previously-known pulsars were also detected.

2.2 The Green Bank Drift-Scan Survey

2.2.1 Overview

Our drift-scan pulsar survey was done using the 100-metre Green Bank Telescope (GBT) during 2002-2003. Observations were made at times when the dish needed to be stationary for maintenance that was required for investigation and repair of problems with the azimuth track. We were able to take advantage of unplanned downtime that resulted from unpredictable scheduling due to the maintenance. The data was taken at frequencies of 400, 600 and 800 MHz, depending on which prime-focus receiver happened to be in place at the time of the observation.

Data was taken using the Berkeley-Caltech Pulsar Machine (BCPM) filterbank (see Backer et al. (1997) for a description, and Camilo et al. (2002) for the discovery of the pulsar in the supernova remnant 3C58, the first pulsar discovery made using the BCPM). This provided 4-bit sampling every $72\mu s$ over a bandwidth of 48 MHz split into 96 channels. Due to the drift-scan nature of our survey, we were not able to choose the integration time at each pointing. The integration time for any particular source is given by the *drift time* of the telescope for the declination of the source. This is the amount of time it takes a point source to move through the beam of the telescope on the sky, and can be calculated for any particular observing frequency and declination. See §3.2.1 for a calculation of the drift time for this survey.

2.2.2 Sky Coverage

Figure 2.1 shows the sky coverage of the survey. The total observing time was about 200 hours, and nearly 600 square degrees were covered. The telescope was pointed North as much as possible, so as to cover the largest range of right ascensions. The colours in the figure represent the three observing frequencies. The blue (darkest) strips were observed at 400 MHz; yellow (lightest) strips at 600 MHz; and green (medium) strips at 800 MHz. The survey consisted of 31 scans taken at a variety of declinations, for different lengths of time ranging from 2 to 14.3 hours.
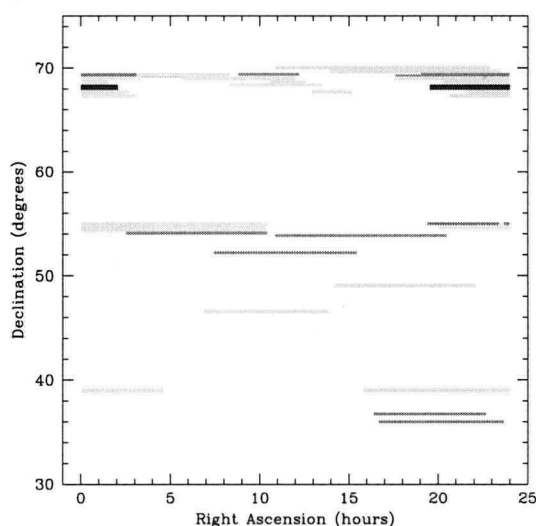
Figure 2.1: The sky coverage for the survey. The colours (grayscale) represent the three observing frequencies: blue (darkest) for 400 MHz; red (lightest) for 600 MHz; and green (medium) for 800 MHz. Declination is plotted versus Right Ascension.

2.2.3 Sensitivity

Our survey is the most sensitive of its kind in this region of the Northern sky. The previous surveys discussed above have a range of sensitivities and sampling times, giving each one a different sensitivity to MSPs. In Table 2.1, the minimum detectable flux and sampling time of our survey is compared with those of the four surveys discussed above. It is clear from

this comparison, especially considering that we sampled at 4 bits as opposed to 1 with the other instruments, that our survey is far more sensitive to MSPs than the others.

The sensitivities in Table 2.1 for our survey were calculated using an expression derived from the radiometer equation (Dicke 1946). The radiometer equation expresses the root-mean-square fluctuations in the system temperature ΔT_{sys} as:

$$\Delta T_{sys} = \frac{T_{sys} + T_{sky}(l,b)}{\sqrt{n_p t_{obs} \Delta \nu}} \tag{2.1}$$

where T_{sys} is the system temperature, $T_{sky}(l,b)$ is the sky temperature for given Galactic coordinates l and b, n_p is the number of orthogonal polarizations sampled, t_{obs} is the integration time, and $\Delta \nu$ is the total bandwidth of the receiver. Using this definition of the RMS noise in the receiver, we obtain (see, for example, Lorimer and Kramer (2004)) an expression for the minimum detectable flux density S_{min} (Dewey et al. 1985):

$$S_{min} = \beta \frac{(S/N_{min})\,[T_{sys} + T_{sky}(l,b)]}{G\sqrt{n_p t_{obs} \Delta \nu}} \sqrt{\frac{W_e}{P - W_e}} \tag{2.2}$$

in terms of the threshold signal-to-noise ratio S/N_{min} (which we take to be 8), antenna gain G, effective pulse width W_e, period P, and quantization correction factor β. We take $\beta = 1$, following the choice of Camilo et al. (1996b) for their survey which used 3-bit sampling. We include the following contributions in the effective pulse width W_e: the intrinsic pulse width of the pulsar W; the dispersion broadening across a single frequency channel τ_{DM} (given by Equation 1.2); the sampling time of the survey τ_{samp}; and the broadening of a pulse due to interstellar scattering τ_{scatt}. We obtain:

$$W_e = \sqrt{W^2 + \tau_{DM}^2 + \tau_{samp}^2 + \tau_{scatt}^2} \tag{2.3}$$

(Dewey et al. 1985; Lyne and Graham-Smith 1998). Both τ_{samp} and τ_{scatt} are assumed to be small in comparison to W and τ_{DM}. This is clear for the sampling time (which is at least an order of magnitude smaller than the fastest pulsar), and the scattering broadening can be expressed as a function of DM and frequency as:

$$\tau_{scatt} = \left(\frac{DM}{1000}\right)^{3.5} \left(\frac{400}{\nu_{MHz}}\right)^4 seconds \tag{2.4}$$

This relation was discovered empirically by Slee et al. (1980; eg, Lyne and Graham-Smith 1998). It can be seen from this expression that for our survey, which is is concerned with DMs smaller than 1000 and frequencies greater than or equal to 400 MHz, we obtain a very small value for τ_{scatt}. This reduces Equation 2.3 to:

$$W_e = \sqrt{W^2 + \tau_{DM}^2} = \sqrt{W^2 + \left[8.3 \times 10^3 \frac{DM}{\nu_{MHz}^3} \Delta\nu \; sec\right]^2} \qquad (2.5)$$

Note that the sky temperature $T_{sky}(l, b)$ is low off the Plane, but it is high on Plane (Haslam et al. 1982). The sensitivities in Table 2.1 and in Figure 2.2 (discussed below) represent the off-Plane best-case scenario, and must be modified when pointing near the Plane.

For our observations, two polarizations and the total bandwidth of 48 Hz were used. The system temperature and gain for each receiver were obtained from the GBT website, and are shown in Table 2.2. The integration times are also listed in the table, as calculated in §3.2.1 for a declination δ. We chose $\delta = 45°$ in Equation 2.1 to obtain the sensitivities in Table 2.1. Note that we calculated the sensitivity of our (100-m) GBT survey only; the values for the other surveys were found in the literature.

Survey	Frequency (MHz)	Sampling Time (μs)	Sensitivity to MSPs (mJy)
Jodrell Bank	411	300	5
Cambridge	81.5	768	200
Green Bank (92-m)	390	5555	2**
Green Bank (43-m)	370	256	8
Green Bank (100-m)	400	72	1.5
	600	72	1.1
	800	72	0.7

Table 2.1: A comparison of the sensitivities of four previous surveys of the Northern sky with our own. Listed are the frequency, sampling time, and minimum detectable flux for each of the surveys. A high sampling rate and a high sensitivity are both required for detecting faint MSPs. ** Note: The minimum flux density for the 92-m Green Bank survey is listed here for normal pulsars; the survey was not sensitive to MSPs.

In Figure 2.2 we plot the minimum detectable flux density at each of our observing

Receiver Frequency (MHz)	T_{sys} (K)	Gain (K/Jy)	Integration Time (sec)
450	57	2.0	$126/\cos\delta$
600	48	2.0	$84/\cos\delta$
800	25	2.0	$63/\cos\delta$

Table 2.2: A table of values required in the sensitivity calculation for the drift scan survey. The values for T_{sys} and the gain were obtained from the GBT website *http://www.nrao.edu//GBT/proposals/proposers_guide/GBTPROPOSERSGUIDE.pdf*, and the integration time is calculated from Equation 3.2.1.

frequencies as a function of pulse period for five different dispersion measures. We assumed an integration time equal to the drift time for each frequency and a declination of 45°. We also assumed a duty cycle of 30% for periods less than 10 ms, and scaled the duty cycle as $P^{-1/2}$ for periods greater than 10 ms. This choice of a period-dependent pulse width was used in Cordes et al. (2005, submitted), which describes the ALFA pulsar survey being performed with the Arecibo Observatory. Equation 2.2 was used to produce the plots, using the information in Table 2.2. Pulse broadening due to dispersion smearing is included in the total pulse width W.

2.3 Expectations

A survey covering 1.8 sr of the Northern sky was performed at 390 MHz using the 92-m Green Bank telescope (Dewey et al., 1985). We use the results from this survey to obtain a very rough estimte of the number of pulsars that we expect to detect in the portion of sky covered by our drift-scan survey. Their observing frequency of 390 MHz is not significantly different from the frequencies used in our survey ($\sim$ 400, 600, 800 MHz), so we have not attempted to correct for changes in flux at different frequencies due to pulsar spectral indices (typically $\sim$ 1.6 (Lorimer et al. 1995)). With a sensitivity of $S_{min} \sim$ 2 mJy, Dewey et al. detected 83 pulsars in $\sim$ 5909 square degrees. Based on our sky coverage of 591 square degrees, this number of pulsars scales to $\sim$9. However, our sensitivity is $\sim$ 1 mJy. In order to estimate the scaling factor due to this difference in sensitivity, we need to make an assumption about the distribution of pulsars in the sky. Assuming a minimum detectable flux density S_{min}, and that the number of detectable pulsars is limited by luminosity rather
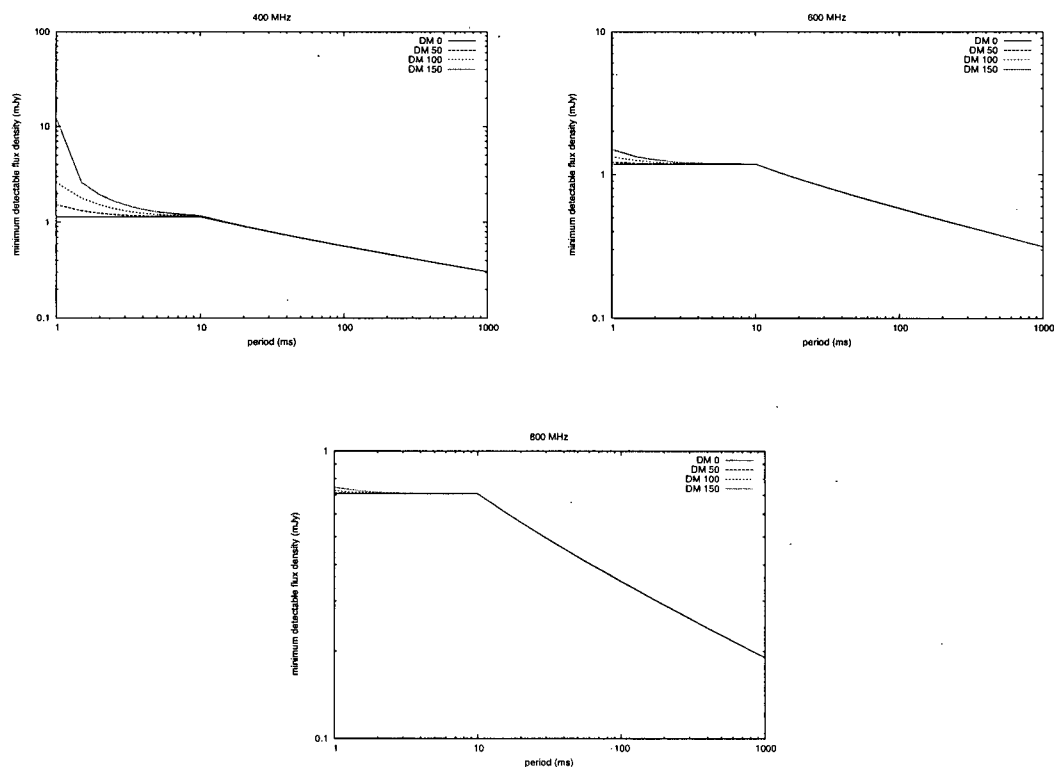
Figure 2.2: The minimum detectable flux density (in mJy, log scale) versus the pulse period in milliseconds, for 400, 600 and 800 MHz. A range of dispersion measures is plotted for each frequency. A duty cycle of 30% is assumed for periods less than 10ms, and the duty cycle is scaled as $W \propto P^{-1/2}$ for periods P greater than 10 ms. Pulse broadening due to dispersion smearing is included.

than scattering, we make two independent calculations, based on a planar distribution and an isotropic distribution of pulsars. If we assume a planar distribution, the number of pulsars should scale as $N \propto S_{min}^{-1}$, and we should expect $\sim (\frac{1mJy}{2mJy})^{-1} = 2$ times the number of pulsars per square degree in our survey than in the 390 MHz survey. If we assume an isotropic distribution of pulsars, the number of pulsars should scale as $N \propto S_{min}^{-3/2}$. We would therefore expect to detect a factor of $\sim (\frac{1mJy}{2mJy})^{-3/2} = 2.8$ times more pulsars than the 390 MHz survey. This is about 18 - 25 pulsars in all. Since we know of 5 pulsars that should be detectable in our survey, this leaves $\sim$ 13 - 20 new pulsars left for us to discover in our data. We expect that one or two of these will be MSPs, based on the overall fraction of MSPs in the population of known pulsars (eg, Hobbs et al. 2004). Note that this is a very rough estimate of the number of pulsars we should see in our survey, and it also does not account for the RFI in our survey, which has made detections more difficult. A full analysis would require a pulsar population model covering all Galactic latitudes, recognizing that pulsars are not really isotropically distributed but instead have different scale heights for young and millisecond pulsars. It would also take into account the fact that we used multiple frequencies in our survey.

Chapter 3

Data Reduction: Searching

Here we will describe the process through which the drift-scan data was reduced. The standard search procedure was followed (as described in §3.1), and the specific considerations needed in dealing with the drift-scan data will be addressed. We will discuss the organization of the data as well as specifics about searching using the signal processing software package `sigproc`. The `sigproc` package, written by Duncan Lorimer, and incorporating his `seek` software, is publically available from *http://www.jb.man.ac.uk/~drl/sigproc*.

3.1 Search Procedure

The central problem in searching for pulsars is to find a periodic signal with unknown period, an unknown dispersion measure, and an unknown amplitude and pulse width, within a time series containing seemingly random noise. The two main parameters in our search space are the dispersion measure and the period of the pulsar. There have been many techniques and algorithms developed that aid in at efficiently detecting signals that are buried within a time series. Some of the methods used in the drift-scan survey are discussed here.

3.1.1 Dedispersion

The process by which a pulsar signal is dispersed by the interstellar medium is discussed in §1.1.2. The effect is only visible due to the pulsed nature of the pulsar signals, and can be seen in a plot of observing frequency versus the time-of-arrival of a particular pulse (see Figure 3.1). Although it is possible to completely correct for dispersion through a process called *coherent dedispersion* (Hankins and Rickett 1975), during pulsar searches it is not necessary for a time series to be perfectly dedispersed in order to detect a pulsar signal. We therefore use dedispersion techniques that are more efficient, both in storage and computing time, when searching for pulsars.

Conceptually, the simplest method of dedispersing a time series $x_{i,j}$ (sampled at frequency channel i and time sample j) is to apply the appropriate time delay to each frequency channel. This is the method of dedispersion performed in our survey using `sigproc`. If we have N frequency channels, and ν_i is the centre frequency (in MHz) of the ith channel, then the time delay of a dispersed signal with dispersion measure DM, relative to the first channel is (according to Equation 1.1):

$$\Delta t_i = \frac{1}{2.41 \times 10^{-4} s^{-1}} \times \left(\nu_1^{-2} - \nu_i^{-2}\right) \cdot DM \qquad (3.1)$$

The number of time samples by which the ith channel must be shifted is then $k_i = \frac{\Delta t_i}{t_{samp}}$, so we can write the dedispersed time series as (Hankins and Rickett 1975):

$$y_j = \sum_{i=1}^{N} x_{i,j-k_i} \qquad (3.2)$$

Although this method is conceptually simple, it is not always the most computationally efficient algorithm. An algorithm that can in some cases be much more efficient was developed by Taylor (1974), and is referred to as tree dedispersion. It requires $N log_2 N$ computations, as opposed to the N^2 computations required for the simple dedispersion process described above; however, it is not always optimal for all surveys, due to additional steps involved and assumed linearity of the signal with frequency. Tree dedispersion will not be discussed any further here, as it was not used in the analysis of our survey.

3.1.2 Periodicity Searches

Once we have a dedispersed time series, it can be searched for periodic signals. This can be done in either the time domain or the frequency domain. Our searches were done in the frequency domain. Within `sigproc` we used `find`, which applies a Fast Fourier Transform on the dedispersed time series and performs a periodicity search in the frequency domain. If a Fourier amplitude of a particular spectral bin (of width $1/t_{obs}$) is above a given signal-to-noise threshold, the centre frequency of the bin is recorded as a periodicity. Since the number of samples in each time series is unlikely to be a power of two (which is convenient for performing Discrete Fourier Transforms), the technique of zero padding is used in our survey. This constitutes the addition of zero-valued samples at the end of our time series, and can also be useful in increasing the number of spectral bins and decreasing the bin
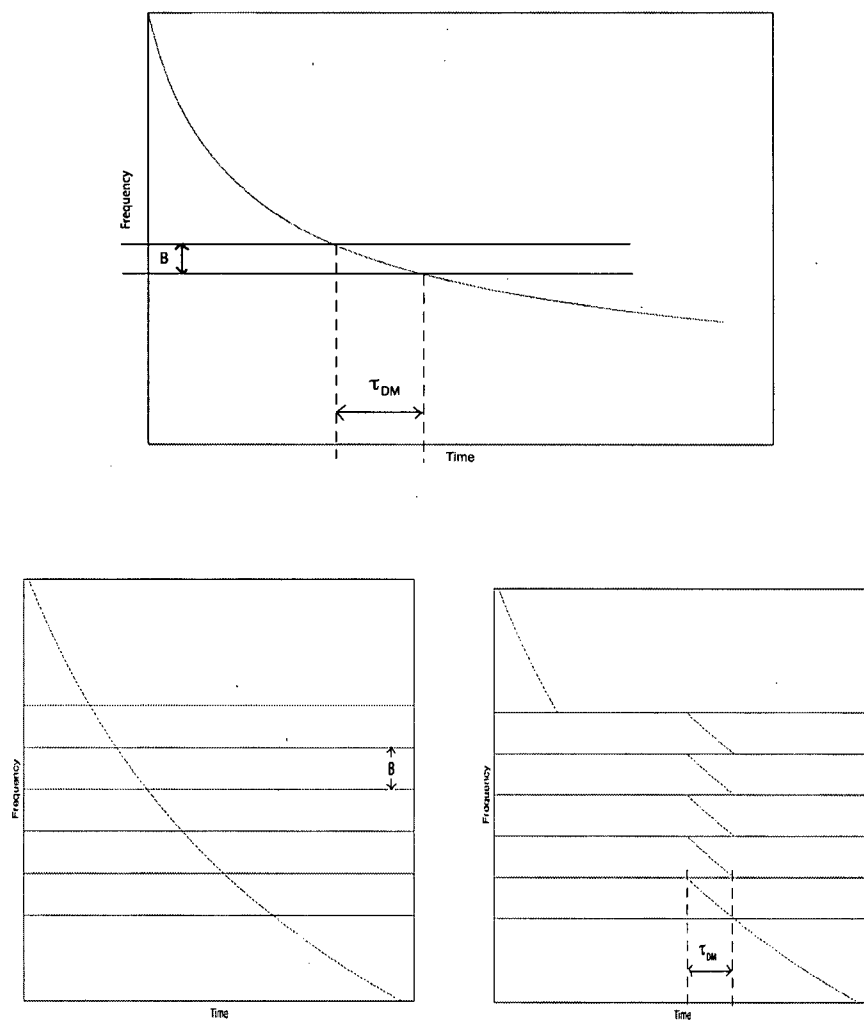
Figure 3.1: Top: Frequency channel versus the time of arrival of two consecutive pulses. The time delay within one frequency channel (of width B) is illustrated. Bottom, left: Our total bandwidth is split up into many smaller frequency channels. Bottom, right: We introduce a time delay to each channel, which is dependent on the centre frequency of the channel, relative to the centre frequency of the lowest frequency channel, as well as the DM of the pulsar. For a total of N frequency channels, this can increase the signal-to-noise of the pulse by a factor of $\sqrt{N}$.

size. A feature of zero padding is that it is less likely for a periodicity to fall between two neighboring bins, thereby splitting its power between the two bins and lowering its signal-to-noise. See Lorimer and Kramer (2004) for more details on frequency-domain searching.

Harmonic Summing

During this stage of the pulsar signal processing, harmonic summing is performed to better detect narrow pulses. For pulses with large duty cycles, their pulse shape is more nearly sinusoidal than those with very narrow duty cycles. A pulse that is nearly sinusoidal will require fewer Fourier components to describe it, and so its Fourier power in the fundamental will be stronger than that of a narrow pulse, which has its Fourier amplitudes split between several components. It is for this reason that we consider five harmonic folds. The process of harmonic summing sees the original spectrum stretched by a factor of two, and then its amplitude added to that of the original spectrum. The same occurs for the second, third and fourth harmonic folds. In the `find` algorithm, the first, 2nd, 4th, 8th and 16th harmonics are summed together. The idea here is to add up the Fourier components that are strongly harmonically related, so as to reduce any bias towards pulsars with larger duty cycles. Summing up to 16 harmonics suffices for duty cycles as low as 2%; however, for pulses that are narrower summing to 32 harmonics may improve the sensitivity (eg, Ransom et al. 2002; Taylor and Huguenin 1969).

Acceleration Searching

One other consideration that is often used in searching for binary pulsars in short orbits is an acceleration search. The need for a search in orbital acceleration is clear when searching for short-orbital period binaries within long integrations. The acceleration due to the orbital motion of the binary system often causes the the topocentric period of the pulsar to vary so much that the signal-to-noise of the pulsar is dramatically decreased. This can cause such a pulsar to go undetected, if the signal-to-noise is reduced to a value below the detection limit. Within `find` there is the option of including an acceleration search. The program searches for signals using a list of trial acceleration values, and outputs a list of signal-to-noise values for each acceleration value in the list. Although we are searching for systems that are potentially short-orbit binaries, the option to search in acceleration space was not used. The first reason for this is that this particular search is so computationally intensive

that it is best used in long-integration globular cluster searches, in which the dispersion measure is already known, which eliminates the need to search a large range of DMs. A second reason is that for this drift scan, the integration times are typically between one and five minutes, which we reasonably assume to be short compared to the orbital period of the binary systems we are looking for. We do not expect a significant decrease in signal-to-noise due to binary motion.

3.2 Data Reduction: Searching

3.2.1 Drift Time Calculation

In a drift-scan survey, an important consideration is the fact that the telescope does not track a particular position on the sky, but stays stationary while allowing the sky to move through its beam. The *drift time* is the amount of time that a point source at a particular declination will remain in the beam of the telescope for a given observing frequency. This is the amount of time we would expect to be able to see a pulsar. Most of the drift times in our survey are on the order of a few minutes, while each scan is a few hours long. If we were to search each entire scan for periodicities, we would not expect to detect a signal from a pulsar that is visible for such a small portion of the time. We therefore need to split the whole observation into smaller pieces of length equal to the drift time. Each small piece can be searched for periodicities.

To calculate the drift time, we need to consider first the apparent angular speed of a source on the sky, and also the size of the beam on the sky. In order to calculate the apparent speed of a source at a given declination δ, we must first consider that the beam of the telescope does not sweep out an equal amount of sky solid angle at each declination. This is illustrated in Figure 3.2: the apparent path of a source on the sky throughout one Earth rotation is greater for declinations closer to zero. In fact, the apparent angular distance traveled throughout one day by a source at a declination of zero degrees is

$$\theta(\delta = 0) = 2\pi. \tag{3.3}$$

To obtain the angular distance traveled by a source at any declination δ, we scale Equation
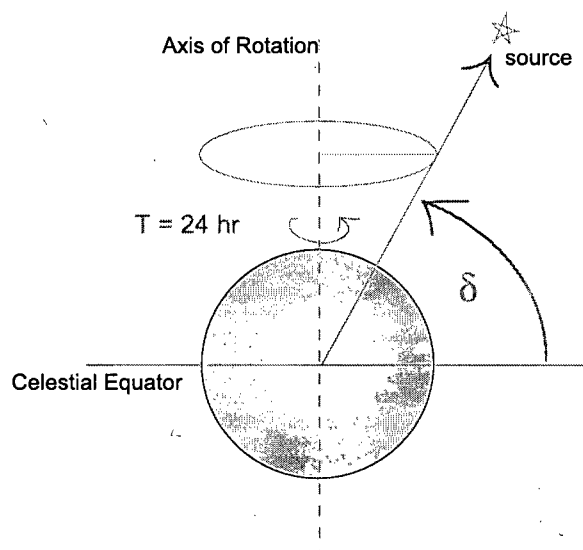
Figure 3.2: An illustration of the path swept out by a source at declination δ during one Earth rotation. Notice that this apparent path scales as $\cos \delta$ with declination.

3.3 by $\cos \delta$, so that

$$\theta(\delta) = 2\pi \cos \delta. \tag{3.4}$$

Now, since the corresponding period is 24 hours, we can write:

$$\omega = \frac{2\pi \cos \delta}{24 \ hr} = \frac{\cos \delta}{4} \ arcmin/sec \tag{3.5}$$

Because the GBT is a radio telescope, its beamwidth is diffraction-limited . The beamwidth is therefore frequency-dependent, and is given on the GBT website ($http://www.nrao.edu/GBT/proposals/short\_guide/introduction.html$) by

$$B = \frac{740 \ arcseconds}{\nu_{GHz}} \tag{3.6}$$

for a frequency ν_{GHz} in GHz. The drift time is then

$$t_{drift} = \frac{B}{\omega} = \frac{49,600 \ sec}{\nu_{MHz} \cdot \cos \delta} \tag{3.7}$$

for a frequency ν_{MHz} in MHz. The drift time depends on both the observing frequency and the declination of the source. These two factors are constant throughout any single observation, so that the drift time need only be calculated once per scan.

For each scan, the drift time was calculated according to equation 3.7. Small files (with integration time equal to the drift time) were created using the `filterbank` task in `sigproc`, which convertes the raw BCPM data into a standard filterbank format that can be further processed using other `sigproc` tasks. Each small file was processed individually.

Our goal is to find unknown pulsars within our data, located at unknown positions on the sky. Because we have a drift scan survey, each chunk of data (which corresponds to a particular time interval) corresponds to a particular strip of sky. However, we do not know a priori exactly where a pulsar will be on the sky. For this reason, some consideration needed to be made about how to split up each scan into its many small (drift time - length) files. We decided to overlap the small files by one-half the drift time, so as to minimize the chance of missing a pulsar due to its signal being split between two files. See Figure 3.3 for a schematic of how the scan was split into small files.

Figure 3.3: A schematic explaining how each scan is split up into small files. Our choice to overlap the files by half the drift time effectively doubles the amount of processing required, but minimizes the chance of missing a pulsar due to its signal being split between two files. The colours are used only to differentiate between consecutive files.

3.2.2 RFI Excision

Radiofrequency interference (RFI) can be a substantial problem in pulsar surveys. Many Earth-based periodic signals (such as the AC power line at 60 Hz and broadband television stations) can seem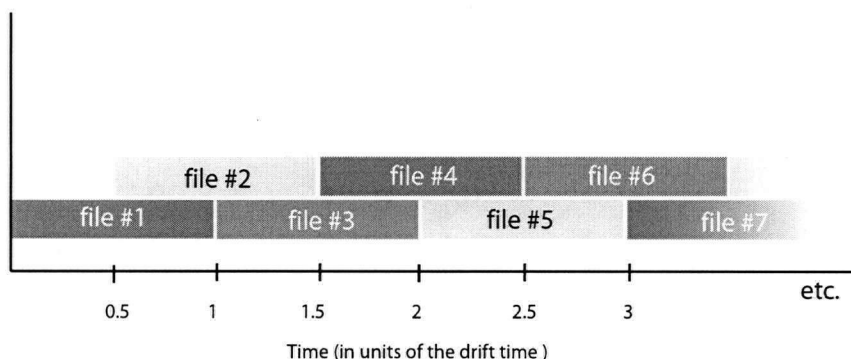 very pulsar-like, and can limit the effectiveness of a survey. RFI costs time (by looking at the RFI instead of other, possibly real, candidates), and often causes real pulsars to go undetected if they are weak or have periods very similar to that of the unwanted signals. It can also have an influence on the spectrum.

In this survey, RFI excision was performed both before and after a time series is searched for periodicities. When excision is done before the searching, the DM zero timeseries is searched for periodicities, and a list of bad signals (often referred to as a *birdies file*, or a *zap list*) is compiled. It is useful to excise RFI before the search for several reasons. First, it reduces the total RMS of the signal, thereby giving any real pulsars a higher total SNR. Second, it can prevent signals that are known a priori to be bad from swamping candidate lists in later stages of data analysis. Looking at the RFI before the searching takes place also gives a good indication of which signals can be expected to appear in the candidate lists. Since the birdies list itself need not contain all bad signals (in some cases, zapping all bad signals could result in a large percentage of the spectrum being removed!), the bad signals not included in the birdies list will likely appear in the final candidate lists. In such a case, it is useful to have a prior list of signals present in the data so as not to waste time further analyzing these signals. RFI filtering after the search process can also be very useful. We take advantage of the fact that we are looking at multiple positions on the sky at different times, and cross-examine all signals detected within one scan. This screening process significantly decreases the number of human hours required in looking at pulsar candidates. Both of these types of RFI filtering are discussed in the following sections.

Pre-search Filtering

Fortunately, it is possible to identify a large amount of RFI relatively easily. Terrestrial sources of RFI are usually detected by `sigproc` with a DM of zero. A broadband signal that is emitted from the Earth does not become significantly dispersed by the time it reaches our receiver. The time delay between two frequencies within our bandwidth (Equation 1.1) will be small so that any dispersion effects will not be noticeable. In pulsar searching, it is

is therefore useful to create a time series that has been dedispersed at a DM of zero and to inspect it for periodic signals.

Any periodicities found in the DM zero time series are most likely RFI. The signals found in the DM zero time series are put into a list called a *birdies* file. This is a list that specifies which spectral bins to zap during the search process. We specify the central frequency to be zapped, the width of the channel to be zapped, as well as the number of harmonics of each signal to be zapped. Careful analysis was performed to enter the correct pulse width and number of harmonics. An analysis of the DM zero time series was performed for all scans using both `sigproc` and another pulsar signal processing software package, PRESTO (written by Scott Ransom (Ransom, 2001), and publicly available from http://www.cv.nrao.edu/~sransom/presto/). `sigproc` was used to obtain a list of periodicities present in the DM zero time series, and PRESTO's `explorefft` was used to obtain information about the frequency width and the number of harmonics to be zapped. Not zapping enough of the spectrum can allow the signal from a true pulsar to be swamped by RFI; however, zapping too much spectrum has the danger of ignoring spectral bins that contain the pulse frequency of a true pulsar.

For the drift-scan survey, an additional measure was taken to assure that the signals in the DM zero timeseries are indeed RFI and not nearby pulsars. In a drift scan, the telescope is continuously looking at different pointings throughout an observation. As a result, a time series covering more than a few drift times should not yield any true candidates. A real pulsar should only be visible for one drift time, and over a longer time series its signal should become diluted so as to produce no real candidates. Therefore, a relatively long DM zero timeseries should detect any persistent RFI present during that portion of the observation.

The drift-scan survey consisted of 31 scans taken at different declinations and frequencies, for different lengths of time ranging from 2 to 14.3 hours (see Table 4.1). Because each scan was different, this required a different birdies file to be created for each scan. The time variation of RFI within one scan was monitored, and it appears that the RFI does not vary much over the course of a single scan. The assumption was therefore made that the RFI did not change significantly within each observation of this drift-scan survey, so that one birdies file was sufficient for a large portion of a scan. The first half hour of each observation was used to represent the RFI within that entire observation (except for the longest observations, for which two or more birdies files were required). The DM zero timeseries of the first half hour of data is formed and searched for periodicities. The resulting periodicities are placed

into the birdies file.

One last consideration during the pre-search RFI excision is to ignore specific frequency channels from our bandpass. The idea here is to eliminate any specific channels that consistently receive strong RFI. A preliminary attempt was made at characterizing the RFI as a function of the bandpass. However, this did not prove to be simple: the bandpass changed drastically with time for the scans that were analyzed, and we were not able to find a clear consistent association between any particular channel(s) and the strong RFI. Further investigation continues, as we hope to create an automatic system for zapping specific channels within our bandwidth.

Post-Search Filtering

Once the searching process is finished for a given scan, the next step is to look at each candidate plot by eye to determine how likely it is that the candidate is a pulsar. However, there are typically anywhere from hundreds to thousands of candidates that result from a single scan. Not only is this time consuming for the individual who must look through each candidate, but it is also not efficient. In looking through each candidate, there are certain things that we look for in determining how interesting the candidate is. The most obvious consideration is a quick glance at the candidate's period. If a signal of exactly the same period is detected in several different regions of the sky, it is probably of terrestrial origin.

A script called `filter` was written to compare each candidate to all other candidates within a scan. Only the candidates that 'passed' the conditions set by `filter` were allowed on to the next stage of the candidate selection process (see §4). `filter` allows a candidate to 'pass' if its period is significantly different (i.e. to ~ 4 decimal places) from all but 5 other candidates. We give preference to periods which are detected in adjacent beams. We here define two beams to be *adjacent* if they are either overlapping (eg, files #1 and #2 in Figure 3.3) or consecutive (eg, files #1 and #3 in Figure 3.3). If the candidate's period is detected in at least one adjacent beam, we then allow for up to 10 other candidates to have the same period. The choice of the number of similar periods allowed for a candidate was somewhat arbitrary, but it is based on the fact that a true pulsar should appear in 3 or 4 (assuming that the pulsar does not happen to fall exactly into one of the arbitrarily chosen drift time segments) beams: two adjacent beams, and one or two overlapping beams. The post-processing period filtering has eliminated many false candidates that appear in

multiple pointings, and has also been successful in allowing the known (re-detected) pulsars to be easily detected.

Another filter that allowed for a significant drop in the number of bad candidates was to place a lower limit on the period of the pulsar candidates. The number of sub-millisecond candidates that appeared in the candidate lists was astounding, and most of these candidates were not convincing and were often barely detections at all. We therefore decided to place a lower cutoff at one millisecond, so as to eliminate any sub-millisecond detections. This adds the danger of eliminating some interesting pulsars, but is much more efficient.

A final technique that was used in the drift-scan survey was to eliminate unwanted signals through consideration of the DM smearing across a channel. This is done once the candidate lists have been produced. Pulsars emit radiation at a broad range of wavelengths. Dispersion (see §1.1.2) causes the pulses from higher frequency emission to reach us slightly earlier than those at lower frequencies. Dedispersion corrects for this effect; however, the pulse is still smeared over a certain time interval τ_{DM} given by equation 1.2:

$$\tau_{DM} = 8.3 \times 10^3 \frac{DM}{\nu_{MHz}^3} \Delta\nu \ sec$$

Therefore, any signals with period less than τ_{DM} will have a significant decrease in sensitivity due to this smearing effect. Therefore, if the period of each candidate is compared with the value of τ_{DM} for that particular observation, any candidate having period less than τ_{DM} can be dismissed as an interesting candidate. Although this particular filter was performed for all candidates, the elimination of all sub-millisecond pulsar candidates (see above) generally made this filter redundant.

3.2.3 DM List

Once the observation has been split into small segments as in §3.2.1, the next step is to decide, for each segment, the DM's at which it will be dedispersed and searched. The DM list is defined by two values: the *maximum DM* and the *DM step* . The maximum DM is the highest dispersion measure at which we would expect to be able to detect a pulsar. Since the dispersion measure depends on the amount of gas that lies between us and the pulsar, a model of the galaxy must be used for a reasonable estimation of the maximum DM along a given direction. The Galactic coordinates are calculated for each pointing, and

the maximum DM is determined using the NE2001 Galactic Free Electron Density Model (Cordes and Lazio 2002) given those coordinates. The DM step is the space between two consecutive DMs at which the timeseries will be dedispersed and searched. It is important to choose a DM step appropriate for the observation. If too large a step is used, then a pulsar with a DM somewhere between two trial values in the list may have its pulse broadened too much to be detected. If too small a step is used there is a danger of performing many redundant calculations, as the dedispersed timeseries of two consecutive DMs may not be significantly different. A compromise can be made between the need for sufficient resolution in DM and the desire to limit computing requirements. This can be found by setting the time delay between the outermost frequency bands (as given by equation 1.2) equal to the sampling time of the survey. The resulting DM step is given by (eg, Lorimer and Kramer 2004):

$$\Delta DM = 1.205 \times 10^{-7} cm^{-3} pc \; t_{samp} \times \frac{\nu^3}{\Delta \nu} \tag{3.8}$$

with sampling time t_{samp}, centre frequency ν, and bandwidth $\Delta \nu$ in MHz.

Although the values of the maximum DM and DM step described above are reasonable choices, it was desirable in the drift-scan survey to use a larger maximum DM, and a smaller DM step, thereby increasing the total number of trial DMs by a factor of 9. This increased both the range and resolution in DM. The increased range (typically searching DMs in the range from 0 to 120 $pc \; cm^{-3}$) gave us confidence that we were not missing pulsars by not searching to high enough DMs. The higher resolution in DM allowed the SNR versus DM plot to be a better diagnostic tool. A plot of SNR versus DM can help to distinguish whether or not the candidate is a pulsar (see §3.2.5 and §3.2.6). The search algorithm (§3.2.4) included a script called hunt which searched for periodicities at each trial DM, and then recorded each such detection into a file. However, each periodicity found by hunt was not necessarily detected at all DMs: weaker periodicities were often detected only at a few dispersion measures. The SNR versus DM plot could consequently only deliver a limited amount of information. Increasing the total number of trial DMs provides opportunity for more detections and therefore better resolution in the plot. See §3.2.6 for a description of further attempts at improving the diagnostic plots.

3.2.4 Searching

In §3.2.1, it is explained how one observation (scan) is split up into small sections which are converted into filterbank format. Each of the small filterbank files must go through the searching stage independently, and a master candidate list is compiled from a combination of the results from the individual files. I will here consider just one of the small files, and explain how it is searched for periodicities.

In order to search for periodicities in the data, several sigproc tasks are called into action. The process for a single drift-time length filterbank file is as follows:

- Given a dispersion measure, a time series is created by introducing the appropriate delay to each frequency channel through dedisperse. See §1.1.2 for more details on dedispersion.

- find zero-pads and fourier-transforms the time series created by dedisperse and searches for significant features in the frequency domain. The raw spectrum as well as the first four harmonic folds (see §3.1.2) are searched. For every harmonic fold, the period and SNR is stored for each detected signal.

- In order to easily create a list of dispersion measures to search at (see §3.2.3), step is used. Given a DM range and a DM step, a DM list is created.

- *hunt* automates the search process by iterating dedisperse and find for each trial dispersion measure in the DM list. find produces a list of detections for each trial DM, all of which are collected into one file.

- A list of the best overall candidates is created using best. It looks at the output from find, and after calculating how the signals are harmonically related, decides which signals appeared the strongest in that particular observation. The candidates are listed in order of decreasing SNR.

3.2.5 Folding

Once the time series has been searched for periodicities, each detection can be folded and inspected by eye. The folding algorithm used by fold in sigproc is a basic one. For a

given time series and pulse period, the pulse phase is calculated for each time sample, and the sample is placed in the corresponding phase bin. The result is a time series that is folded modulo a given period. The script which automates the folding of the best signals resulting from a search is called `foldsignals`. The `foldsignals` script obtains a list of all candidates produced by `best` and creates a dedispersed time series at the detected DM. Since it is important to know the period extremely precisely, `foldsignals` proceeds to fold the time series at 64 periods in a narrow range about the period initially detected by `find`, and chooses the best period to be the one which gives the highest SNR upon folding. The time series is separated into eight sub-bands, and is also separated into eight sub-integrations. This information is all used by `sigproc`'s plotting program `quickplot` which gives an output as in Figure 3.4.

The `quickplot` output can then be inspected by eye for specific features that are characteristic of pulsars. Some such features are:

- The folded time series should have a clear peak

- Ideally, the peak should appear at the same phase for all sub-bands and all sub-integrations. If it appears in only one sub-band, odds are that it is RFI. If the signal appears in only one sub-integration, then it was not on during the entire observation. It is possible that such a signal is from a nulling pulsar, or it could be a pulsar that is just not completely in this beam (considering the transiting nature of this survey). However, if this same signal does not appear in adjacent beams, this could mean that the signal is due to RFI. Signals that are found in overlapping (or adjacent) beams are given some preference over those that appear only once.

- There should be a clear peak in the plot of SNR versus DM. This is because the pulse becomes significantly broadened when the DM is not close enough to the true DM of the pulsar, thus lowering the peak SNR of the signal. A signal that peaks at zero DM is likely RFI.

The above are guidelines that were followed in inspecting the detections for pulsars. Any interesting signals that met some number of the above criteria were saved as candidates and the search was refined.

3.2.6 Refining the Search Parameters

Finally, once a good list of candidates has been created based on the folded plots, a more intense search can be performed to further refine the search parameters. A search is performed in a grid of DM and period, and a plot is created from the period and DM producing the highest SNR. The value of this search is two-fold. First, the search refines the DM and period, thereby allowing for a higher peak SNR in the folded time series, and hence, more confidence in the classification as either a true detection, false detection, or RFI. Second, the two-parameter grid is plotted in greyscale and used as a final diagnostic as to whether or not the signal is pulsar-like. A true pulsar will exhibit a peak in the two-dimensional space, probably close to the centre of the space (depending on how good the original detection was). A false detection will likely show no distinct pattern, and RFI will peak at zero DM.

In order to refine the search, a modified `quickplot` program was written. This modified program was called `quickgrid`, which has a similar output to `quickplot`, but with a greyscale DM-period grid replacing the non-folded time series. The gridding algorithm is similar to that used in the ATNF program `pdm`, which also performed a two-dimensional search in period and DM. See Figure 3.4 for a sample output of `quickgrid`.

The ranges of period and DM over which to search were chosen in the following way. The search in period follows that used in `foldsignals`, using a range determined by the observation time. The range of periodicities searched is $\left(\frac{1}{p_{mid}} - \frac{1}{t_{obs}}\right)^{-1}$ to $\left(\frac{1}{p_{mid}} + \frac{1}{t_{obs}}\right)^{-1}$ where p_{mid} is the period of the detected signal and t_{obs} is the length of the observation (drift time). The number of trial periods can be specified, but for most purposes of the drift-scan survey, was kept at 64 trial periods (which is the same number of trial periods used in `quickplot`. The range for the DM search is determined by the number of DM trials and the resolution in DM step. The DM step is calculated as in §3.2.3, but is made to be even smaller at this stage, in order to further increase the resolution in DM. For the purposes of this survey, the DM step used was equation 3.8 divided by 30 (a factor of 10 smaller than the original DM step used), and the number of trial DM's was kept at 32. The number of DM steps was chosen to be 32 after having experimented in an attempt to balance between good resolution and limiting the number of iterations required from the CPU-intensive program that produces the plots. When less than 32 DM steps were used,

there was degradation in the resulting plots. However, there did not appear to be much benefit to increasing the number of DM steps above 32.
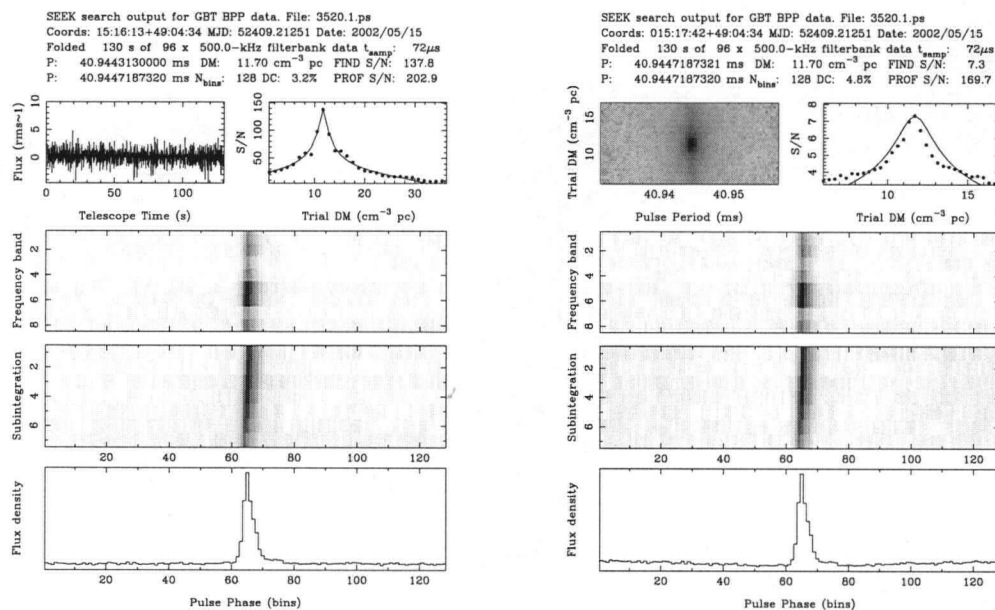
Figure 3.4: Left: An example of the output from `quickplot`. The search information is listed at the top of the plot. The top left plot is the time series. The top right plot is signal-to-noise versus trial DM. The third from the bottom is a plot of signal-to-noise for each of 8 frequency bands versus pulse phase; the second from the bottom is a similar plot for each sub-integration; the bottom plot is the integrated profile. The bottom three plots are shown for the period and DM which maximize the SNR. Right: An example of a plot using `quickgrid`. This is a similar to the `quickplot` output in that the signal-to-noise is maximized in period and DM space, but we here include a grid in period and DM (the top left plot) which can help to diagnose whether a candidate is a pulsar. For a real pulsar, we expect to see the signal-to-noise peak up in both period and DM as is seen here. Both plots were created using data from J1518+4904, a pulsar that was re-detected in our survey.

Chapter 4

Results: Candidates

As of the writing of this thesis, 24 of the 31 scans have been processed. Table 4.1 is a list of the scans by observation date, and shows each scan's declination and right ascension range. The focus of this section is the overall list of candidates that was produced by the search code. The classification scheme used in ranking the candidates will be discussed, and tables of both new candidates and re-detected pulsars will be presented. However, a recently-discovered bug in the `foldsignals` code that produces the diagnostic plots has made it necessary for us to reproduce these plots using a corrected version of `foldsignals` for all candidates. This will significantly change the classification of many candidates, requiring that we re-evaluate our classification system. We have reproduced the plots for a subset of the data that was initially processed (the non-bold scans in Figure 4.1), and will present some Class 1 candidates that resulted.

4.1 Classification System

In order to organize the tens of thousands of detections that resulted from the drift-scan survey, a classification system was required. It was necessary to keep track of which were good pulsar candidates that should be followed up, and which are probably not worth looking at again. We have successfully proposed to re-observe good candidates for confirmation, while Class 4 candidates are considered false detections, and will not be studied any further. The following sections describe the classification system in more detail, and give some examples of Class 1 candidates.

4.1.1 Class 1 Candidates

Class 1 objects are those that look convincingly like pulsars. These objects appear in two to four adjacent drift times, and do not have a maximum in SNR at a DM of zero. To

Date	Frequency	Declination	RA start	RA end	Scan length	Drift time
mm-dd-yyyy	MHz	dd:mm:ss	hh:mm:ss	hh:mm:ss	hr	sec
05-14-2002	590.00	68:24:10	08:15:20	13:31:12	5.3	232
05-15-2002	590.00	49:04:34	14:16:19	22:02:36	7.8	130
06-04-2002	575.00	70:00:00	13:54:06	22:55:35	9.0	256
06-05-2002	575.00	69:40:00	13:58:02	00:30:24	9.5	252
06-08-2002	820.00	69:23:00	08:48:55	12:11:59	3.4	174
06-09-2002	820.00	69:23:00	19:02:36	06:34:29	11.5	174
06-13-2002	820.00	69:15:00	17:37:18	05:39:16	12.0	173
06-29-2002	570.00	69:20:00	03:05:45	08:21:37	5.3	250
07-04-2002	570.00	69:00:00	17:33:27	03:20:03	9.8	246
07-04-2002	590.00	69:00:00	05:35:25	11:59:48	6.4	238
07-07-2002	590.00	46:33:29	05:12:18	12:13:27	7.0	124
07-08-2002	590.00	68:40:00	10:34:42	12:35:01	2.0	234
07-09-2002	590.00	68:40:00	20:16:59	01:32:41	5.3	234
07-10-2002	590.00	70:00:00	10:52:22	13:52:52	3.0	249
07-18-2002	410.00	68:10:00	19:05:34	01:38:18	6.5	330
07-29-2002	590.00	67:40:00	21:38:15	02:39:04	5.0	224
08-06-2002	590.00	67:20:00	20:36:57	03:08:01	6.5	221
08-06-2002	590.00	67:40:00	12:55:06	15:10:28	2.3	224
08-07-2002	590.00	39:00:04	13:10:44	01:57:49	12.8	109
10-12-2002	820.00	54:59:10	14:27:27	18:28:06	4.0	107
10-13-2002	820.00	54:59:10	18:42:35	22:43:15	4.0	107
10-13-2002	**820.00**	**54:59:10**	**00:45:25**	**03:15:15**	**4.0**	**107**
10-15-2002	820.00	54:59:10	21:53:52	04:24:56	6.5	107
10-17-2002	**570.00**	**54:58:55**	**19:49:56**	**05:28:21**	**9.6**	**154**
10-17-2002	**570.00**	**54:38:46**	**15:17:10**	**05:36:11**	**14.3**	**152**
10-21-2002	570.00	54:19:23	20:59:56	05:53:53	8.9	151
10-22-2002	820.00	54:04:17	22:08:20	06:02:07	7.9	104
03-20-2003	**800.00**	**52:12:00**	**07:24:49**	**15:26:08**	**8.0**	**102**
03-21-2003	**820.00**	**53:50:00**	**06:36:29**	**16:12:42**	**9.6**	**104**
06-03-2003	**800.00**	**36:45:00**	**16:25:00**	**22:40:00**	**~6.3**	**76.7**
06-06-2003	**800.00**	**36:00:00**	**16:40:00**	**23:40:00**	**~7.0**	**76.0**

Table 4.1: A list of all observations in the drift-scan survey. The first column shows the date of the observation; the second column is the observing frequency; the third column is the declination of the strip; the fourth and fifth columns are the right ascensions at the beginning and end of the scan; next is the length of the scan, and the last column is the drift time for each scan's frequency and declination, as calculated by Equation 3.7. Those in bold font are scans that are yet to be processed.

Period (ms)	DM ($cm^{-3}pc$)	Detected SNR	Coordinates RA+Dec	Drift Time (sec)	Flux Density (mJy)
1083.12898	5.30	8.1 (13.2)	22:19:00+69:00:00	246	1
620.739771	22.40	9.2 (36.3)	07:40:09+69:00:00	246	2

Table 4.2: A list of two Class 1 candidates from the survey. The detected period, dispersion measure, and coordinates are shown. The flux densities are estimated from the radiometer equation, and are very rough estimates because we do not know if the pulsars were centered in the telescope beam.

be in this category, the candidate should have enough signal for it to be clear that they are true signals and not random noise added in such a way as to produce a signal-to-noise ratio above the threshold. Figure 3.4 shows the *foldsignals* and *quickgrid* outputs for the test pulsar, PSR 1518+4904, and shows a clear, strong pulsar-like folded profile as well as a peak in both DM and period. The next step for a Class 1 candidate is a follow-up observation using the GBT.

We have thus far detected two Class 1 candidates, which are listed in Table 4.2 and shown in 4.1. It will be necessary to rerun `foldsignals` on all Class 3 and Class 4 candidates. This will likely increase the number of Class 1 and Class 2 candidates.

4.1.2 Class 2 Candidates

Class 2 candidates are those that appear like pulsars, but which are either too weak to be able to confidently classify as a Class 1, or for which there is some reason to cast doubt on its pulsar status. The next step for Class 2 candidates is to refine the search as in §3.2.6 using *quickgrid*. If the refined search increases confidence that it is a pulsar, the candidate will be promoted to Class 1. If it is still not clear that it is a pulsar but it still looks promising, the candidate will remain in Class 2. If the candidate looks worse upon refining the search, the candidate may move down to either Class 3 or Class 4.

4.1.3 Class 3 Candidates

Class 3 candidates are those that are probably either false detections or RFI, but which may still be of interest. One or more of the criteria in §3.2.5 must have been met; usually, either the integrated profile or the DM plot has a peak, but some of the other criteria are
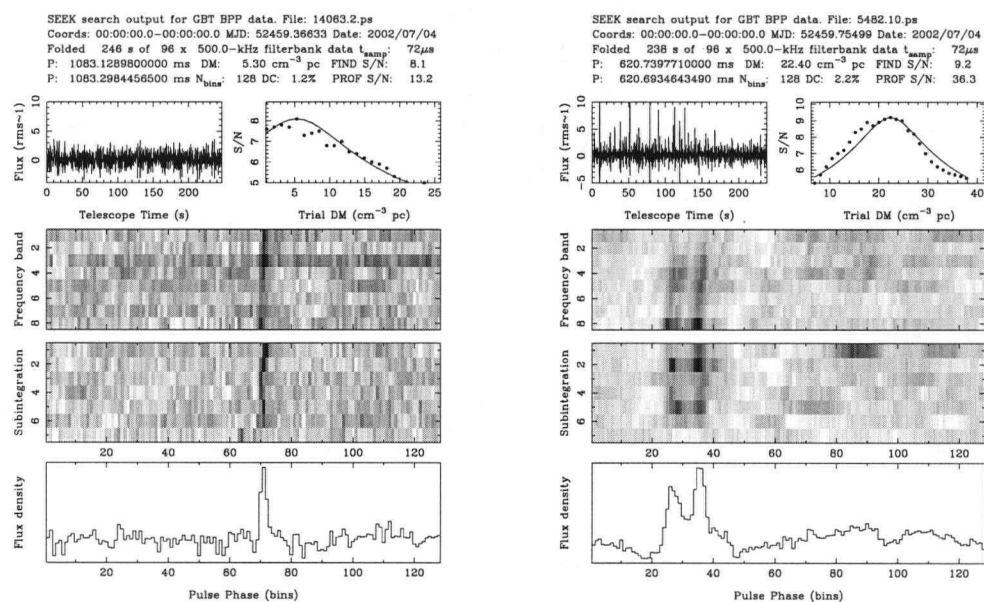
Figure 4.1: `quickplot / foldsignals` output for two Class 1 candidates. See Table 4.2 for more information about the candidates.

Name	Observing Frequency (MHz)	Known Period (ms)	Known DM $(cm^{-3}pc)$	Known Coords (J2000) RA+Dec	Flux Density (mJy)
B0105+68	590	1071.07252	61.092	01:08:30+69:05:53	< 2.1
B0329+54	570	714.48373	26.833	03:32:59+54:34:44	1337
B0329+54	820	714.48373	26.833	03:32:59+54:34:44	550
B0355+54	820	156.38242	57.153	03:58:54+54:13:14	20
J1518+490	590	40.94456	11.6109	15:18:17+49:04:34	8.7
B2241+69	575	1664.46403	40.74	22:42:56+69:50:52	1.6

Table 4.3: A list of the known pulsars that were in the region of sky processed to date in our survey. The topocentric period, DM, J2000 coordinates, flux density and predicted SNR of the pulsars are listed here. The observing frequency of the scan in which each pulsar would have been observable is listed as well. The flux densities listed correspond to these frequencies. The DMs and coordinates were obtained from the ATNF pulsar catalogue. The periods were estimated using the known ephemeris of each pulsar with TEMPO. Flux density measurements were obtained from Stairs et al. 1999 (J1518+4904), Lorimer et al. 1995 (B0105+68,B0329+54, B0355+54, B2241+69), interpolating between measured values when necessary. The predicted SNR was calculated using Equation 2.2 along with the fluxes listed in this table. Pulsars discovered by Dewey et al. 1985 (B0105+68, B2241+69), Cole and Pilkington 1968 (B0329+54), Manchester et al. 1972 (B0355+54) and Nice et al. 1996 (J1518+4904). B2241+69 was not detected as it lies at the edge of two of the observed declination ranges.

Name	Observing Frequency MHz	Detected Period (ms)	Detected DM $(cm^{-3}pc)$	Detected Coords (J2000) RA+Dec	SNR	Flux Density (mJy)
B0105+68	590	1071.00485[1]	67.4[2]	01:08:04+69:00:00	9.4	1.8
B0329+54	570	714.46733	40.6[3]	03:33:01+54:19:23	247.2	7.9
	820	714.53173	31.61	03:31:58+54:04:17	19.6	0.54
B0355+54	820	156.37017	57.44	003:58:14+54:04:17	84.46	11.6
J1518+4904	590	40.94431	11.7	15:17:42+49:04:34	121.47	12.3

Table 4.4: Previously known pulsars, re-detected in the drift-scan survey. Shown here are the period, DM, coordinates, SNR and predicted flux density of the pulsars as found by this survey. The SNR is the signal-to-noise ratio calculated from profiles dedispersed and folded at the known DM and topocentric period of the pulsar. Note that B0329+54 was detected in two separate scans of this survey, and so two sets of search parameters are given here. Both of these detections were made while B0329+54 was *outside* of the beam of the telescope, which explains the decreased flux as compared with that listed in Table 4.3. [1] B0105+68 was detected at its second harmonic, with period 535.50243 ms. [2]The offset between the DM listed here and the known DM in Table 4.3 is due to the fact that the observing frequency in the header file being used was incorrect by 20 MHz. [3]We had multiple detections of B0329+54 with a range of DMs. The plot in Figure 4.2 has a clear slope in sub-bands plot, indicating that the detected DM is incorrect.

SEEK search output for GBT BPP data. File: 24179.4.ps
Coords: 01:08:04+69:00:00 MJD: 52459.48341 Date: 2002/07/04
Folded 246 s of 96 x 500.0-kHz filterbank data t_{samp}: 72μs
P: 535.5024250000 ms DM: 67.40 cm^{-3} pc FIND S/N: 8.5
P: 535.5412678280 ms N_{bins}: 128 DC: 3.1% PROF S/N: 14.2

SEEK search output for GBT BPP data. File: 6974.70.ps
Coords: 03:31:07+54:18:23 MJD: 52568.19032 Date: 2002/10/21
Folded 151 s of 96 x 500.0-kHz filterbank data t_{samp}: 72μs
P: 714.3463010000 ms DM: 40.60 cm^{-3} pc FIND S/N: 11.4
P: 714.4673334380 ms N_{bins}: 128 DC: 24.0% PROF S/N: 269.9

SEEK search output for GBT BPP data. File: 5185.1.ps
Coords: 03:58:14+54:04:17 MJD: 52569.21119 Date: 2002/10/22
Folded 104 s of 96 x 500.0-kHz filterbank data t_{samp}: 72μs
P: 156.3701740000 ms DM: 58.40 cm^{-3} pc FIND S/N: 86.6
P: 156.3778158530 ms N_{bins}: 128 DC: 6.0% PROF S/N: 245.1

SEEK search output for GBT BPP data. File: 3520.1.ps
Coords: 15:16:13+49:04:34 MJD: 52409.21251 Date: 2002/05/15
Folded 130 s of 96 x 500.0-kHz filterbank data t_{samp}: 72μs
P: 40.9443130000 ms DM: 11.70 cm^{-3} pc FIND S/N: 137.6
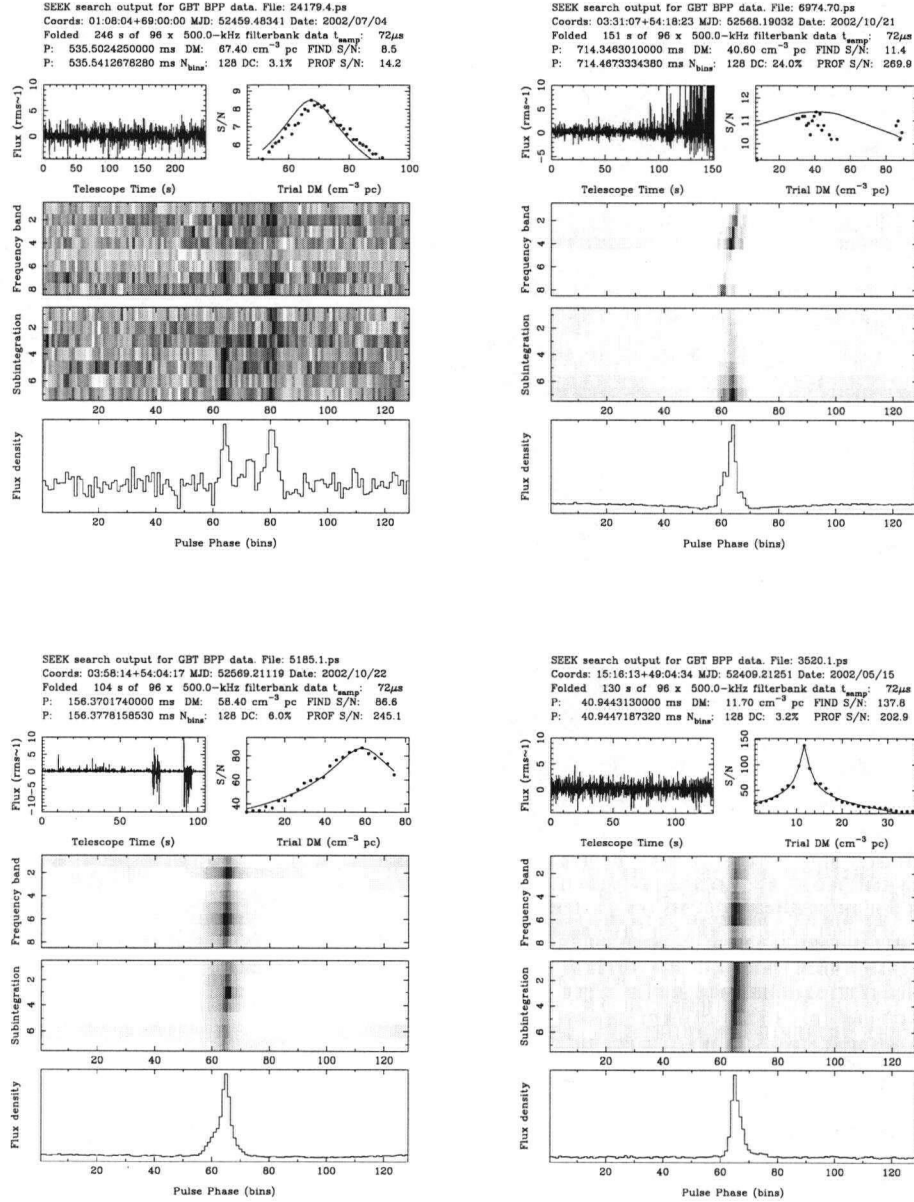P: 40.9447187320 ms N_{bins}: 128 DC: 3.2% PROF S/N: 202.9

Figure 4.2: Detection plots for the re-detected pulsars. Top left: B0105+68; Top right: B0329+43; Bottom left: B0355+54; Bottom right: J1518+4904. There was a second detection of B0329+54 with a lower SNR at 820 MHz. Note that the SNR-DM plot is strange in the B0329+54 plot, since it has two peaks in DM. This probably occurred due to saturation by the strong signal, and also by the fact that there appears to be significantly more signal in some sub-bands than others.

not met. Often, interesting candidates that appear to be RFI are initially classified as Class 3, just in case they turn out to be pulsars. As with Class 2 objects, the search for a Class 3 candidates is refined in DM and period. Typical results from refining the search for a Class 3 candidate have either proven the candidate to be uninteresting, or to be a source of terrestrial RFI.

4.1.4 Class 4 Candidates

Class 4 objects are unlikely to be pulsars. In the survey results, many of the 'candidates' found by `sigproc` have been either persistent RFI (often accompanied by many harmonics), or random noise that has been folded in such a way that it appears to have a periodicity. Once a signal is decided to belong to Class 4, it is no longer considered to be a pulsar candidate, and it is no longer studied. The search is not refined on these candidates. A list of Class 4 objects was not compiled, since there are too many such candidates and because they are not considered interesting. However, we will take a fresh look at these candidates with the revised version of `foldsignals`.

4.2 Redetections

There are five previously-known pulsars in the sky area processed to date (listed in Table 4.3). A good check of whether our software and method are working properly is to determine whether or not these were redetected. Four of the previously-known pulsars (B0105+68, two separate detections of B0329+54, B0355+54, and J1518+4904) were re-detected in the survey. Table 4.4 provides the period, DM and SNR of the pulsars as found by the search software. Also included here are the SNR of the detected pulsars, folded at the known DM and topocentric period, and the flux density in mJy, derived from the integrated profiles and the radiometer equation.

We performed a blind search with the drift-scan survey (i.e., the candidate viewing software did not identify previously-known pulsars), which resulted in three of the four detected pulsars having been classified as Class 1 candidates (shown in Figure 4.2). The initial classification of B0105+68 as a Class 3 candidate led to the identification of the error in `foldsignals`. We will reclassify all Class 3 and Class 4 candidates using `foldsignals` now that the software problem is solved.

The pulsar B2241+69 was not detected in the survey; however, this was probably because it was at a declination that lies at the edge of two scans.

Chapter 5

Discussion and Conclusions

5.1   Discussion of Results

The processing of the drift-scan data until now has yielded several re-detections of known pulsars, and has also produced some Class 1 and Class 2 candidates. The small number of convincing new class 1 candidates can be attributed mainly to a recently-corrected software problem within `sigproc` and will increase as more sources are reclassified. The problem in the `sigproc` software had been distorting the integrated profiles of the candidates so that real pulsar signals did not appear as prominent as they should have. This effect has caused real pulsars to receive too low a classification, and has most likely caused real pulsars to go unnoticed. In addition, the RFI that corrupted the data was strongest at 600 MHz, the observing frequency of at least half of our data. Distinguishing real candidates from fake candidates became more difficult due to this prominent RFI.

5.2   Future Work and Conclusions

There are still several prospects for the data. Now that we have identified and fixed the software problem within `sigproc`, a reanalysis of all processed (and unprocessed) scans using an upgraded version of `sigproc` will certainly yield a higher detection rate. The next step is to re-observe the most convincing Class 1 and Class 2 candidates to confirm them as pulsars. We will re-observe some of these candidates with the GBT in December 2005. If a candidate is re-detected at the same location on the sky with a similar period and DM, this is confirmation that the pulsar really exists and was neither a random signal nor some source of RFI. In the case that a candidate is confirmed during the December observations, we will further propose timing observations for the pulsar. A third consideration is to re-examine the data using more sophisticated techniques for RFI excision. For example, if bad channels could be removed systematically, this would improve our chances of detecting

any unknown pulsars. With these future directions, we are optimistic that this drift-scan survey is due to discover some exciting new pulsars.

Bibliography

Alpar, M. A., Cheng, A. F., Ruderman, M. A., and Shaham, J.: 1982, *Nature* **300**, 728

Baade, W. and Zwicky, F.: 1934, *Proc. Nat. Acad. Sci.* **20**, 254

Backer, D. C.: 1970, *Nature* **228**, 42

Backer, D. C.: 1976, *ApJ* **209**, 895

Backer, D. C., Dexter, M. R., Zepka, A., D., N., Wertheimer, D. J., Ray, P. S., and Foster, R. S.: 1997, *PASP* **109**, 61

Backer, D. C., Kulkarni, S. R., Heiles, C., Davis, M. M., and Goss, W. M.: 1982, *Nature* **300**, 615

Callanan, P. J., Garnavich, P. M., and Koester, D.: 1998, *MNRAS* **298**, 207

Camilo, F., Nice, D. J., Shrauner, J. A., and Taylor, J. H.: 1996a, *ApJ* **469**, 819

Camilo, F., Nice, D. J., and Taylor, J. H.: 1996b, *ApJ* **461**, 812

Camilo, F., Stairs, I. H., Lorimer, D. R., Backer, D. C., Ransom, S. M., Klein, B., Wielebinski, R., Kramer, M., McLaughlin, M. A., Arzoumanian, Z., and Müller, P.: 2002, *ApJ* **571**, L41

Camilo, F., Thorsett, S. E., and Kulkarni, S. R.: 1994, *ApJ* **421**, L15

Chakrabarty, D., Morgan, E. H., Muno, M. P., Galloway, D. K., Wijnands, R., van der Klis, M., and Markwardt, C. B.: 2003, *Nature* **424**, 42

Chen, K. and Ruderman, M.: 1993, *ApJ* **402**, 264

Cole, T. W. and Pilkington, J. D. H.: 1968, *Nature* **219**, 574

Cordes, J. M. and Lazio, T. J. W.: 2002, preprint, astro-ph/0207156

Dewey, R. J., Taylor, J. H., Weisberg, J. M., and Stokes, G. H.: 1985, *ApJ* **294**, L25

Dicke, R. H.: 1946, *Rev. Sci. Instrum.* **17**, 268

Drake, F. D. and Craft, H. D.: 1968, *Nature* **220**, 231

Gold, T.: 1968, *Nature* **218**, 731

Gould, D. M. and Lyne, A. G.: 1998, *MNRAS* **301**, 235

Hankins, T. H. and Rickett, B. J.: 1975, in *Methods in Computational Physics Volume 14 — Radio Astronomy*, pp 55–129, Academic Press, New York

Haslam, C. G. T., Stoffel, H., Salter, C. J., and Wilson, W. E.: 1982, *A&AS* **47**, 1

Helfand, D. J., Manchester, R. N., and Taylor, J. H.: 1975, *ApJ* **198**, 661

Hewish, A., Bell, S. J., Pilkington, J. D. H., Scott, P. F., and Collins, R. A.: 1968, *Nature* **217**, 709

Hobbs, G., Manchester, R., Teoh, A., and Hobbs, M.: 2004, in *IAU Symposium*, pp 139–+

Johnston, S. and Bailes, M.: 1991, *MNRAS* **252**, 277

Komesaroff, M. M.: 1970, *Nature* **225**, 612

Kramer, M., Xilouris, K. M., Lorimer, D. R., Doroshenko, O., Jessner, A., Wielebinski, R., Wolszczan, A., and Camilo, F.: 1998, *ApJ* **501**, 270

Lamb, F. K. and Yu, W., in F. A. Rasio and I. H. Stairs (eds.), *Binary Radio Pulsars*

Linares, M., van der Klis, M., Altamirano, D., and Markwardt, C. B.: 2005, *Discovery of kHz QPOs and shifted frequency correlations in the accreting millisecond pulsar XTE J1807–294*, astro-ph/0509011

Lorimer, D. R.: 2001, *Living Reviews in Relativity*, http://www.livingreviews.org/Articles/Volume4/2001-5lorimer

Lorimer, D. R. and Kramer, M.: 2004, *Handbook of pulsar astronomy*, Handbook of pulsar astronomy, by D.R. Lorimer and M. Kramer. Cambridge observing handbooks for research astronomers, Vol. 4. Cambridge, UK: Cambridge University Press, 2004

Lorimer, D. R., Xilouris, K. M., Fruchter, A. S., Stairs, I. H., Camilo, F., Vazquez, A. M., Eder, J. A., McLaughlin, M. A., Roberts, M. S. E., Hessels, J. W. T., and Ransom, S. M.: 2005, *MNRAS* **359**, 1524

Lorimer, D. R., Yates, J. A., Lyne, A. G., and Gould, D. M.: 1995, *MNRAS* **273**, 411

Lyne, A. G. and Graham-Smith, F.: 1998, *Pulsar astronomy*, Pulsar astronomy / Andrew G. Lyne and Francis Graham-Smith. Cambridge, U.K.; New York : Cambridge University Press, 1998. (Cambridge astrophysics series ; 31) ISBN 0521594138

Lyne, A. G. and Manchester, R. N.: 1988, *MNRAS* **234**, 477

Lyne, A. G., Manchester, R. N., Lorimer, D. R., Bailes, M., D'Amico, N., Tauris, T. M., Johnston, S., Bell, J. F., and Nicastro, L.: 1998, *MNRAS* **295**, 743

Manchester, R. N., Taylor, J. H., and Huguenin, G. R.: 1972, *Nature Phys. Sci.* **240**, 74

Nicastro, L., Lyne, A. G., Lorimer, D. R., Harrison, P. A., Bailes, M., and Skidmore, B. D.: 1995, *MNRAS* **273**, L68+

Nice, D. J., Sayer, R. W., and Taylor, J. H.: 1996, *ApJ* **466**, L87

Nice, D. J., Splaver, E. M., Stairs, I. H., Loehmer, O., Jessner, A., Kramer, M., and Cordes, J. M.: 2005, *A 2.1 Solar Mass Pulsar Measured by Relativistic Orbital Decay*, astro-ph/0508050

Pacini, F.: 1967, *Nature* **216**, 567

Pacini, F.: 1968, *Nature* **219**, 145

Phinney, E. S.: 1992, *Phil. Trans. Roy. Soc. A* **341**, 39

Radhakrishnan, V. and Cooke, D. J.: 1969, *Astrophys. Lett.* **3**, 225

Radhakrishnan, V. and Srinivasan, G.: 1982, *Curr. Sci.* **51**, 1096

Rankin, J. M.: 1993, *ApJ* **405**, 285

Ransom, S. M.: 2001, *Ph.D. thesis*, Harvard University

Ransom, S. M., Eikenberry, S. S., and Middleditch, J.: 2002, *Astronomical Journal* **124**, 1788

Richards, D. W. and Comella, J. M.: 1969, *Nature* **222**, 551

Sayer, R. W., Nice, D. J., and Taylor, J. H.: 1997, *ApJ* **474**, 426

Shrauner, J. A., Taylor, J. H., and Woan, G.: 1998, *ApJ* **509**, 785

Slee, O. B., Dulk, G. A., and Otrupek, R. E.: 1980, *Proc. Astr. Soc. Aust.* **4**, 100

Staelin, D. H. and Reifenstein, III, E. C.: 1968, *Science* **162**, 1481

Stairs, I. H.: 2003, *Living Reviews in Relativity* **6**, 5

Stairs, I. H., Faulkner, A. J., Lyne, A. G., Kramer, M., Lorimer, D. R., McLaughlin, M. A., Manchester, R. N., Hobbs, G. B., Camilo, F., Possenti, A., Burgay, M., D'Amico, N., Freire, P. C., and Gregory, P. C.: 2005, *Discovery of Three Wide-orbit Binary Pulsars: Implications for Binary Evolution and Equivalence Principles*, astro-ph/0506188

Stairs, I. H., Lyne, A. G., and Shemar, S.: 2000, *Nature* **406**, 484

Stairs, I. H., Thorsett, S. E., and Camilo, F.: 1999, *ApJS* **123**, 627

Strohmayer, T. E., Zhang, W., Swank, J. H., Smale, A., Titarchuk, L., Day, C., and Lee, U.: 1996, *ApJ* **469**, L9

Taylor, J. H.: 1974, *A&AS* **15**, 367

Taylor, J. H. and Huguenin, G. R.: 1969, *Nature* **221**, 816

Van Der Klis, M., Swank, J. H., Zhang, W., Jahoda, K., Morgan, E. H., Lewin, W. H. G., Vaughan, B., and Van Paradijs, J.: 1996, *ApJ* **469**, L1

van Kerkwijk, M. H., Bergeron, P., and Kulkarni, S. R.: 1996, *ApJ* **467**, L89

Weisberg, J. M., Romani, R. W., and Taylor, J. H.: 1989, *ApJ* **347**, 1030

Wijnands, R., van der Klis, M., Homan, J., Chakrabarty, D., Markwardt, C. B., and Morgan, E. H.: 2003, *Nature* **424**, 44

Wolszczan, A.: 1990, *IAU Circ.* **5073**, 1

Young, M. D., Manchester, R. N., and Johnston, S.: 1999, *Nature* **400**, 848